NUREG/CR-1806
ORNL/NUREG/TM-419

ornl

OAK
RIDGE
NATIONAL
LABORATORY

UNION
CARBIDE

Heavy-Section Steel Technology Program Quarterly Progress Report for July–September 1980

G. D. Whitman R. H. Bryan

Prepared for the U.S. Nuclear Regulatory Commission
Office of Nuclear Regulatory Research
Under Interagency Agreements DOE 40-551-75 and 40-552-75

OPERATED BY
UNION CARBIDE CORPORATION
FOR THE UNITED STATES
DEPARTMENT OF ENERGY

Printed in the United States of America. Available from
National Technical Information Service
U.S. Department of Commerce
5285 Port Royal Road, Springfield, Virginia 22161

Available from

GPO Sales Program
Division of Technical Information and Document Control
U.S. Nuclear Regulatory Commission
Washington, D.C. 20555

NUREG/CR-1806
ORNL/NUREG/TM-419
Dist. Category RF

Contract No. W-7405-eng-26

NUREG/CR--1806

TI85 015926

Engineering Technology Division

HEAVY-SECTION STEEL TECHNOLOGY PROGRAM QUARTERLY PROGRESS REPORT FOR JULY—SEPTEMBER 1980

G. D. Whitman R. H. Bryan

Manuscript Completed — November 21, 1980
Date Published — December 1980

NOTICE This document contains information of a preliminary nature. It is subject to revision or correction and therefore does not represent a final report.

Prepared for the
U.S. Nuclear Regulatory Commission
Office of Nuclear Regulatory Research
Under Interagency Agreements DOE 40-551-75 and 40-552-75

NRC FIN No. B0119

Prepared by the
OAK RIDGE NATIONAL LABORATORY
Oak Ridge, Tennessee 37830
operated by
UNION CARBIDE CORPORATION
for the
DEPARTMENT OF ENERGY

CONTENTS

PREFACE

The Heavy-Section Steel Technology (HSST) Program, which is sponsored by the Nuclear Regulatory Commission is an engineering research activity devoted to extending and developing the technology for assessing the margin of safety against fracture of the thick-walled steel pressure vessels used in light-water-cooled nuclear power reactors. The program is being carried out in close cooperation with the nuclear power industry. This report covers HSST work performed in July through September 1980. The work performed by Oak Ridge National Laboratory (ORNL) and by subcontractors is managed by the Engineering Technology Division. Major tasks at ORNL are carried out by the Engineering Technology Division and the Metals and Ceramics Division. Prior progress reports on this program are ORNL-4176, ORNL-4315, ORNL-4377, ORNL-4463, ORNL-4512, ORNL-4590, ORNL-4653, ORNL-4681, ORNL-4764, ORNL-4816, ORNL-4855, ORNL-4918, ORNL-4971, ORNL/TM-4655 (Vol. II), ORNL/TM-4729 (Vol. II), ORNL/TM-4805 (Vol. II), ORNL/TM-4914 (Vol. II), ORNL/TM-5021 (Vol. II), ORNL/TM-5170, ORNL/NUREG/TM-3, ORNL/NUREG/TM-28, ORNL/NUREG/TM-49, ORNL/NUREG/TM-64, ORNL/NUREG/TM-94, ORNL/NUREG/TM-120, ORNL/NUREG/TM-147, ORNL/NUREG/TM-166, ORNL/NUREG/TM-194, ORNL/NUREG/TM-209, ORNL/NUREG/TM-239, NUREG/CR-0476 (ORNL/NUREG/TM-275), NUREG/CR-0656 (ORNL/NUREG/TM-298), NUREG/CR-0818 (ORNL/NUREG/TM-324), NUREG/CR-0980 (ORNL/NUREG/TM-347), and NUREG/CR-1197 (ORNL/NUREG/TM-370), NUREG/CR-1305 (ORNL/NUREG/TM-380), NUREG/CR-1477 (ORNL/NUREG/TM-393), and NUREG/CR-1627 (ORNL/NUREG/TM-401).

SUMMARY*

1. PROGRAM ADMINISTRATION AND PROCUREMENT

The Heavy-Section Steel Technology (HSST) Program is an engineering research activity conducted by the Oak Ridge National Laboratory (ORNL) for the Nuclear Regulatory Commission (NRC) in coordination with other research sponsored by the federal government and private organizations. The program comprises studies related to all areas of the technology of materials fabricated into thick-section primary-coolant containment systems of light-water-cooled nuclear power reactors. The principal area of investigation is the behavior and structural integrity of steel pressure vessels containing cracklike flaws. Current work is organized into the following tasks: (1) program administration and procurement, (2) fracture mechanics analyses and investigations, (3) investigations of irradiated materials, (4) thermal shock investigations, and (5) pressure vessel investigations.

The work performed under the existing research and development subcontracts is included in this report.

Fourteen program briefings, reviews, or presentations were made during the quarter.

2. FRACTURE MECHANICS ANALYSES AND INVESTIGATIONS

The finite-element computer program NOZ-FLAW has been made operational on IBM computers for several crack geometries. An automatic mesh generator for nozzle-corner flaws was tested successfully, and test problems with internal pressure loading were executed.

At the University of Maryland, specimen tests and examinations are continuing in the study of brittle-to-ductile transition phenomena. The finite-element code SAMCR is being used to study crack propagation and arrest in compact specimens and to analyze the thermal shock experiment TSE-5. The effect of accounting for nonsingular terms in the stress function on the accuracy of K determined from photoelastic experiments is under study with compact tension and wedge-loading specimens.

3. INVESTIGATIONS OF IRRADIATED MATERIALS

Preparations were made to test the remaining Charpy V-notch impact specimens and tensile specimens from the Third 4T-CTS Irradiation Study.

In the fourth HSST Irradiation Series, the irradiation of capsules A and B continued throughout the quarter with excellent temperature control on capsule A. Control of capsule B is good but not quite as good as that of capsule A.

---

*Conversions from SI to English units for all SI quantities are listed on a foldout page at the end of this report.

4. THERMAL SHOCK INVESTIGATIONS

Preparations for the latest thermal shock test TSE-5A were completed, and the test was successfully performed. More extensive pretest materials characterization studies than those performed for the preceeding test were carried out. Test conditions were selected to give a substantially higher expectation of achieving all test objectives. A preliminary posttest evaluation indicates that all objectives were actually realized: a series of initiation-arrest events occurred, arrest in a rising K_I field was achieved, and the effectiveness of warm prestressing was conclusively demonstrated.

5. PRESSURE VESSEL INVESTIGATIONS

In preparation for intermediate vessel test V-8A with the flaw in a low-upper-shelf seam weld, preliminary trial welds were made by a variety of processes and were tested. A particular welding procedure, which produced acceptable impact and tensile properties, was selected for a final trial and more extensive specimen tests.

In the study of feasibility of pressurized thermal shock tests of intermediate vessels, a preliminary analysis of a pressurized thermal shock loading of a flawed nozzle corner was made. This showed that conditions for crack initiation could be attained with a moderate thermal shock with reasonable pressures and temperatures.

HEAVY-SECTION STEEL TECHNOLOGY PROGRAM QUARTERLY PROGRESS REPORT FOR JULY–SEPTEMBER 1980

G. D. Whitman R. H. Bryan

ABSTRACT

The Heavy-Section Steel Technology (HSST) Program is an engineering research activity conducted by the Oak Ridge National Laboratory for the Nuclear Regulatory Commission. The program comprises studies related to all areas of the technology of materials fabricated into thick-section primary-coolant containment systems of light-water-cooled nuclear power reactors. The investigation focuses on the behavior and structural integrity of steel pressure vessels containing cracklike flaws. Current work is organized into five tasks: (1) program administration and procurement, (2) fracture mechanics analyses and investigations, (3) investigations of irradiated materials, (4) thermal shock investigations, and (5) pressure vessel investigations.

A finite-element code for analyzing nozzle-corner cracks is operational. Crack propagation and damping studies are continuing. Two capsules of fracture specimens in the Fourth HSST Irradiation Series are being irradiated. Thermal shock test TSE-5A was conducted successfully. A procedure for producing a satisfactory low-upper-shelf seam in intermediate test vessel V-8A was developed, and facility planning for pressurized thermal shock tests was continued.

---

1. PROGRAM ADMINISTRATION AND PROCUREMENT

G. D. Whitman

The Heavy-Section Steel Technology (HSST) Program, a major safety program sponsored by the Nuclear Regulatory Commission (NRC) at the Oak Ridge National Laboratory (ORNL), is concerned with the structural integrity of the primary systems (particularly the reactor pressure vessels) of light-water-cooled nuclear power reactors. The structural integrity of these vessels is ensured by (1) designing and fabricating them according to standards set by the code for nuclear pressure vessels, (2) detecting flaws of significant size that occur during fabrication and in service, and (3) developing methods of producing quantitative estimates of conditions under which fractures could occur. The program is concerned mainly with developing pertinent fracture technology, including knowledge of (1) the material used in these thick-walled vessels, (2) the flaw growth rate, and (3) the combination of flaw size and load that would cause fracture and thus limit the life and/or operating conditions of this type of reactor plant.

The program is coordinated with other government agencies and with the manufacturing and utility sectors of the nuclear power industry in the United States and abroad. The overall objective is a quantification of safety assessments for regulatory agencies, for professional code-writing bodies, and for the nuclear power industry. Several activities are conducted under subcontracts by research facilities in the United States and through informal cooperative efforts on an international basis. Two research and development subcontracts are currently in force.

Administratively, the program is organized into five tasks, as reflected in this report: (1) program administration and procurement, (2) fracture mechanics analyses and investigations, (3) investigations of irradiated material, (4) thermal shock investigations, and (5) pressure vessel investigations.

During this quarter, 14 program briefings, reviews, or presentations were made by the HSST staff at technical meetings and at program reviews for the NRC staff or visitors.

2. FRACTURE MECHANICS ANALYSES AND INVESTIGATIONS*

2.1. A Computer Program (NOZ-FLAW) for Direct Evaluation of K-Factors for Arbitrarily Shaped Flaws at Pressure Vessel Nozzle Corners

J. W. Bryson B. R. Bass†

This quarter the nozzle-corner-flaw option in the NOZ-FLAW finite-element computer program was made fully operational on the Union Carbide Corporation Nuclear Division (UCCND) computer facility. Several test problems were executed and a draft report[1] of a user's manual for exercising this option was prepared.

NOZ-FLAW requires as few as eight cards of input to automatically generate a finite-element mesh and calculate K-distributions for nozzle-corner flaws. The convenience of limited input, however, introduces certain restrictions or limitations in the current version of the program. The actual configuration analyzed is shown in Fig. 2.1, which has symmetry

*Conversions from SI to English units for all SI quantities are listed on a foldout page at the end of this report.

†Computer Sciences Division, UCCND.

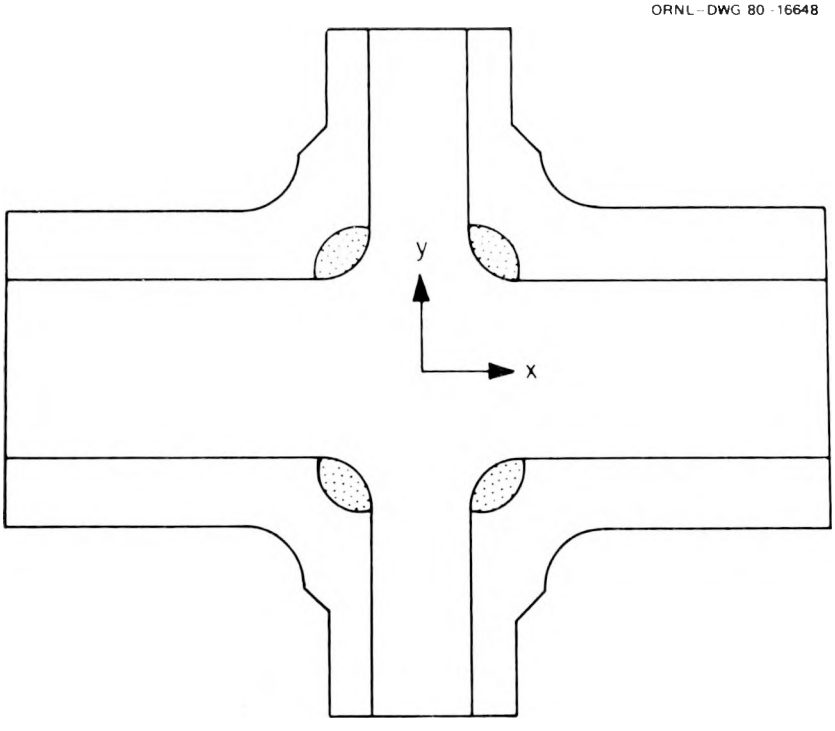

Fig. 2.1. Nozzle-corner flaw configuration with threefold symmetry.

about the x-y, y-z, and x-z planes. Thus, the use of NOZ-FLAW for the analysis of a single nozzle with a single flaw requires an assumption by the analyst that a second nozzle underneath the vessel and the additional flaws introduced do not influence behavior near any one particular flaw. Therefore, use of the present program is recommended only for relatively small diameter nozzles in large diameter vessels. Other limitations include (1) internal pressure loading only, with or without crackface pressure, (2) flaw in longitudinal plane of a standard reinforced nozzle-vessel configuration, and (3) a single linear elastic material.

The intermediate test vessel (ITV) configuration shown in Fig. 2.2 was analyzed using the current NOZ-FLAW program. A quarter-circular flaw (MATH) of depth a = 95 mm and a similar natural flaw (EXPR) obtained in a photoelastic experiment[2] were analyzed under internal pressure loading (100 MPa) with crackface pressure (100 MPa) applied. The quarter-circular flaw was also analyzed under internal pressure loading (100 MPa) without crackface pressure. Figures 2.3 and 2.4 show cross-sectional views of the

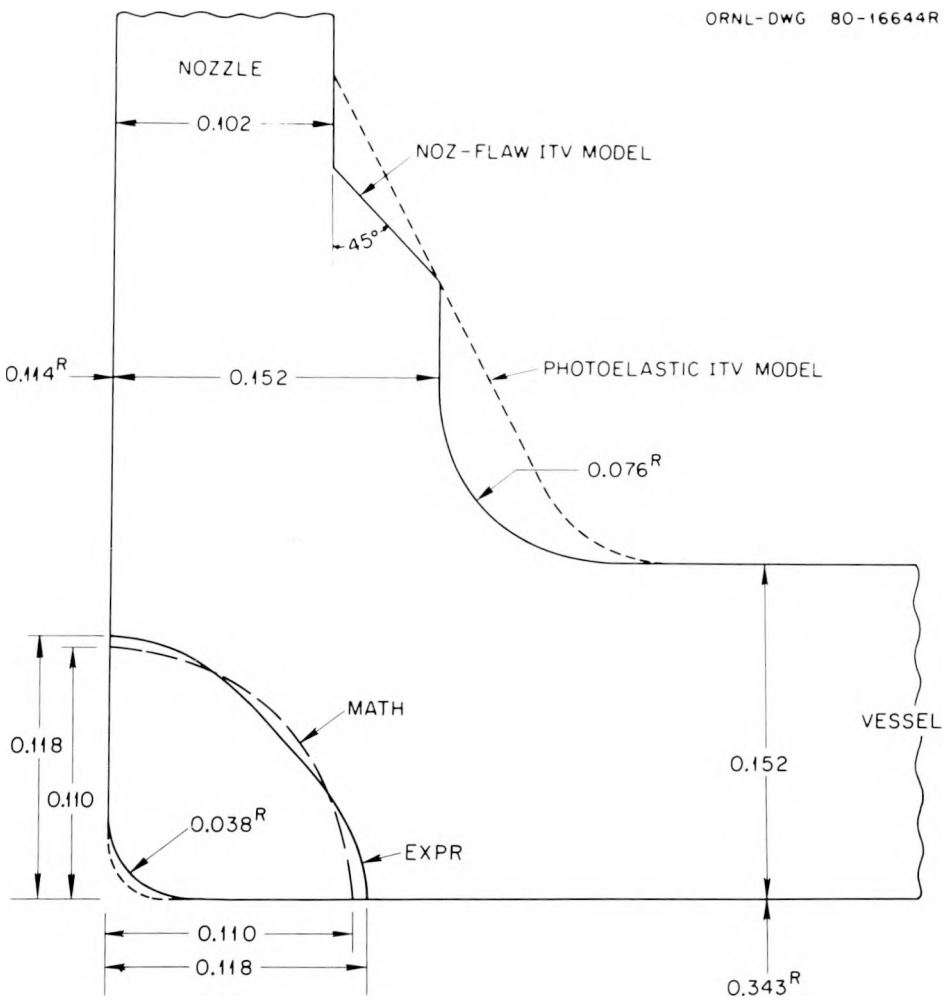

Fig. 2.2. Geometry and dimensions of an ITV configuration.

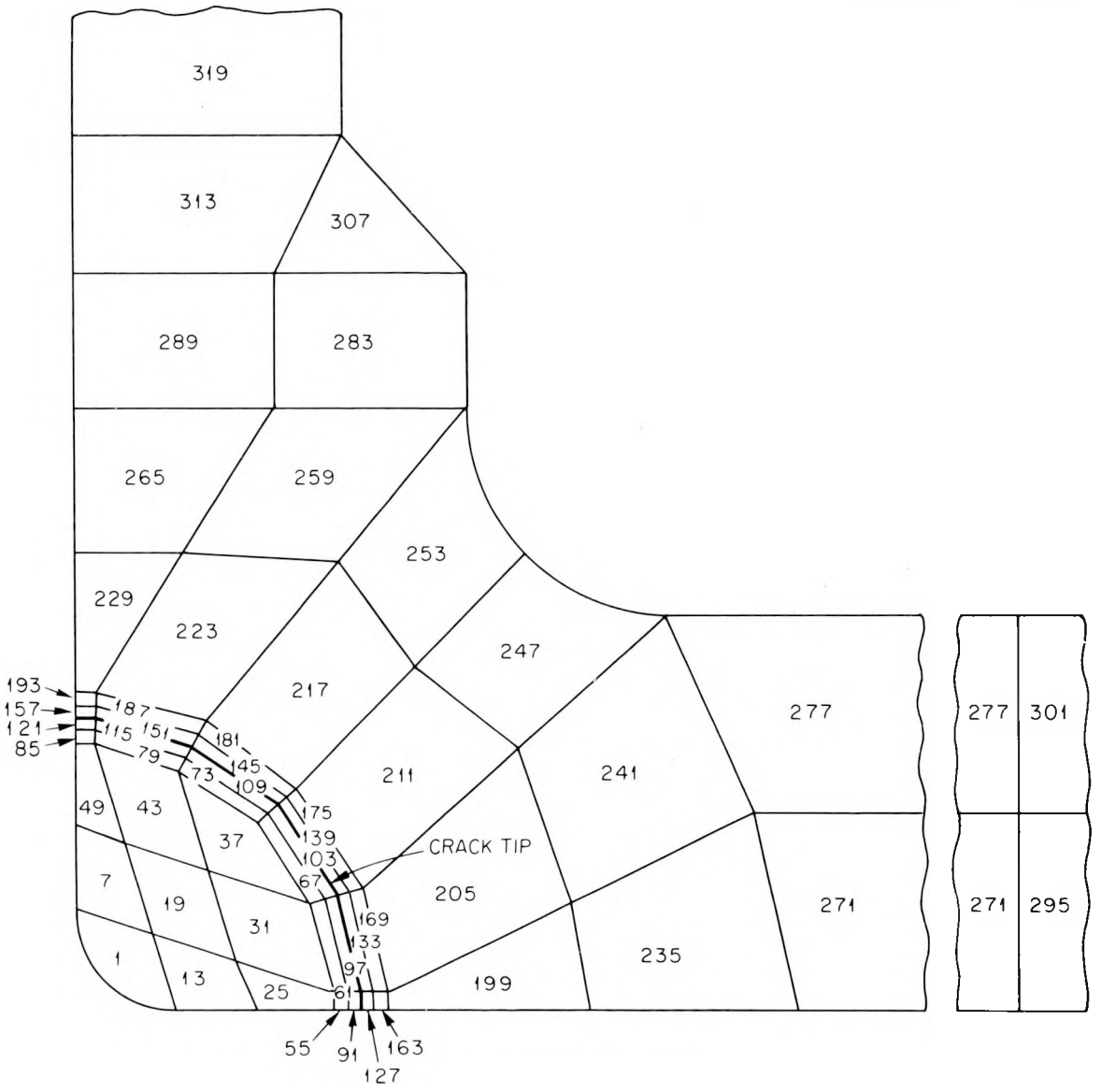

Fig. 2.3. Finite-element discretization for longitudinal plane of ITV model with a quarter-circular flaw (a/w = 0.41, a = 95 mm).

finite-element mesh generated by NOZ-FLAW for the quarter-circular flaw model. Top and side views of the outside surface of the mesh are also given in Figs. 2.5 and 2.6. A total of 324 elements and 1,791 nodes were generated for this model.

The results of the analyses are shown in Fig. 2.7, where normalized K_I values are given at various points along the flaw front. The NOZ-FLAW values plotted were obtained by averaging K-values from corresponding crack-tip elements on each side of the crack tip. In addition, results

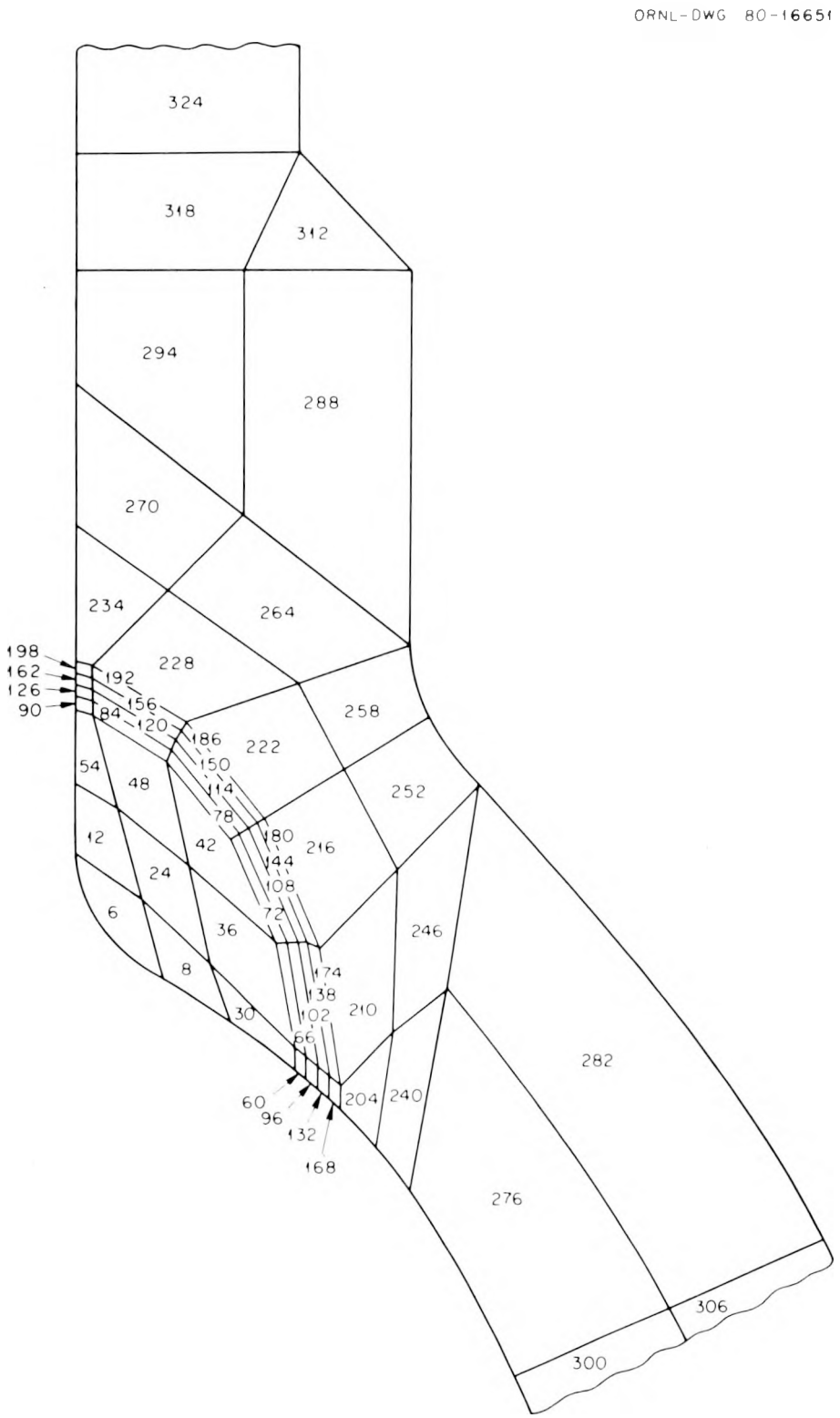

Fig. 2.4. Finite-element discretization for transverse plane of ITV model.

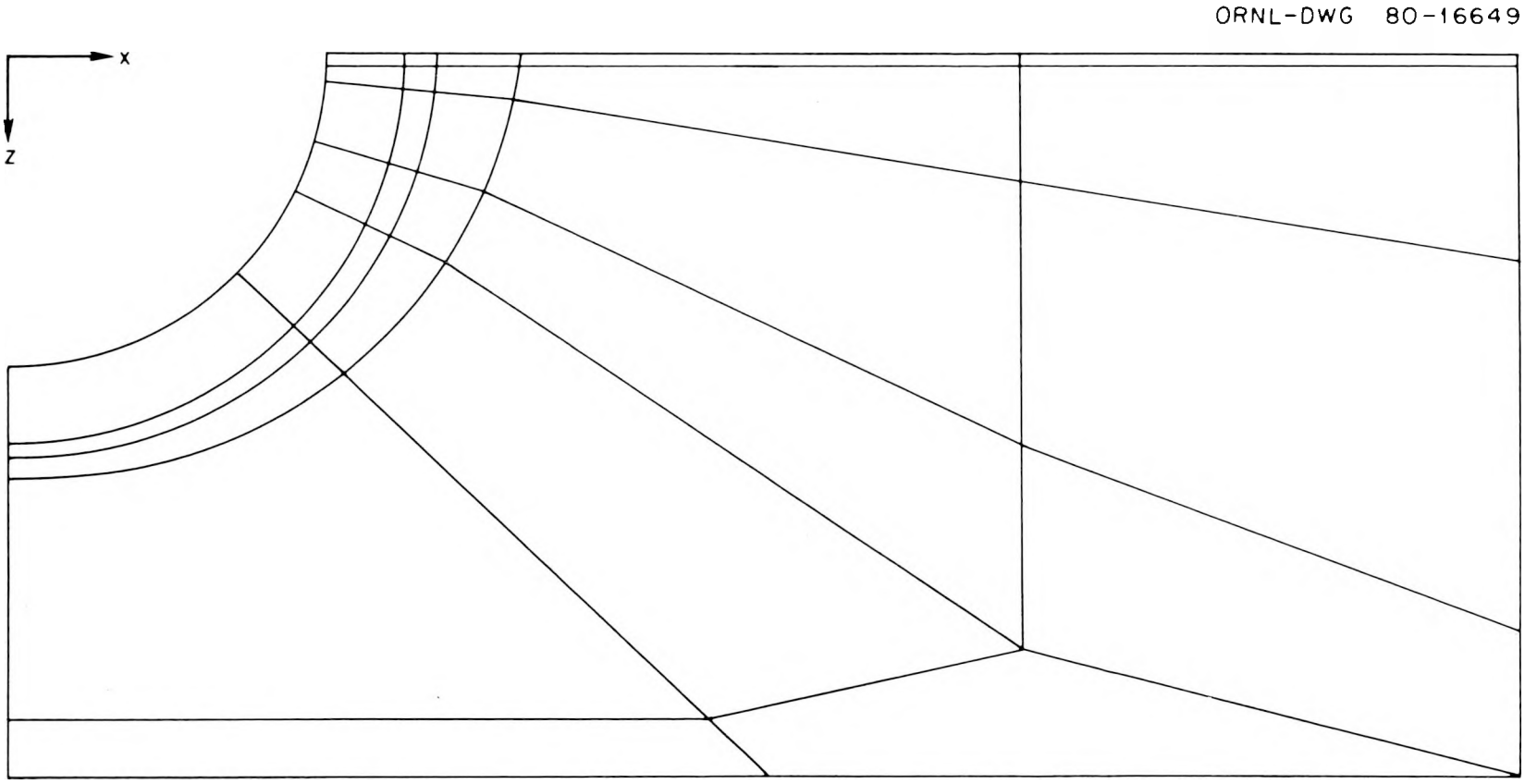

Fig. 2.5. Top view of outside surface of finite-element mesh generated by NOZ-FLAW for ITV configuration.

ORNL-DWG 80-16650

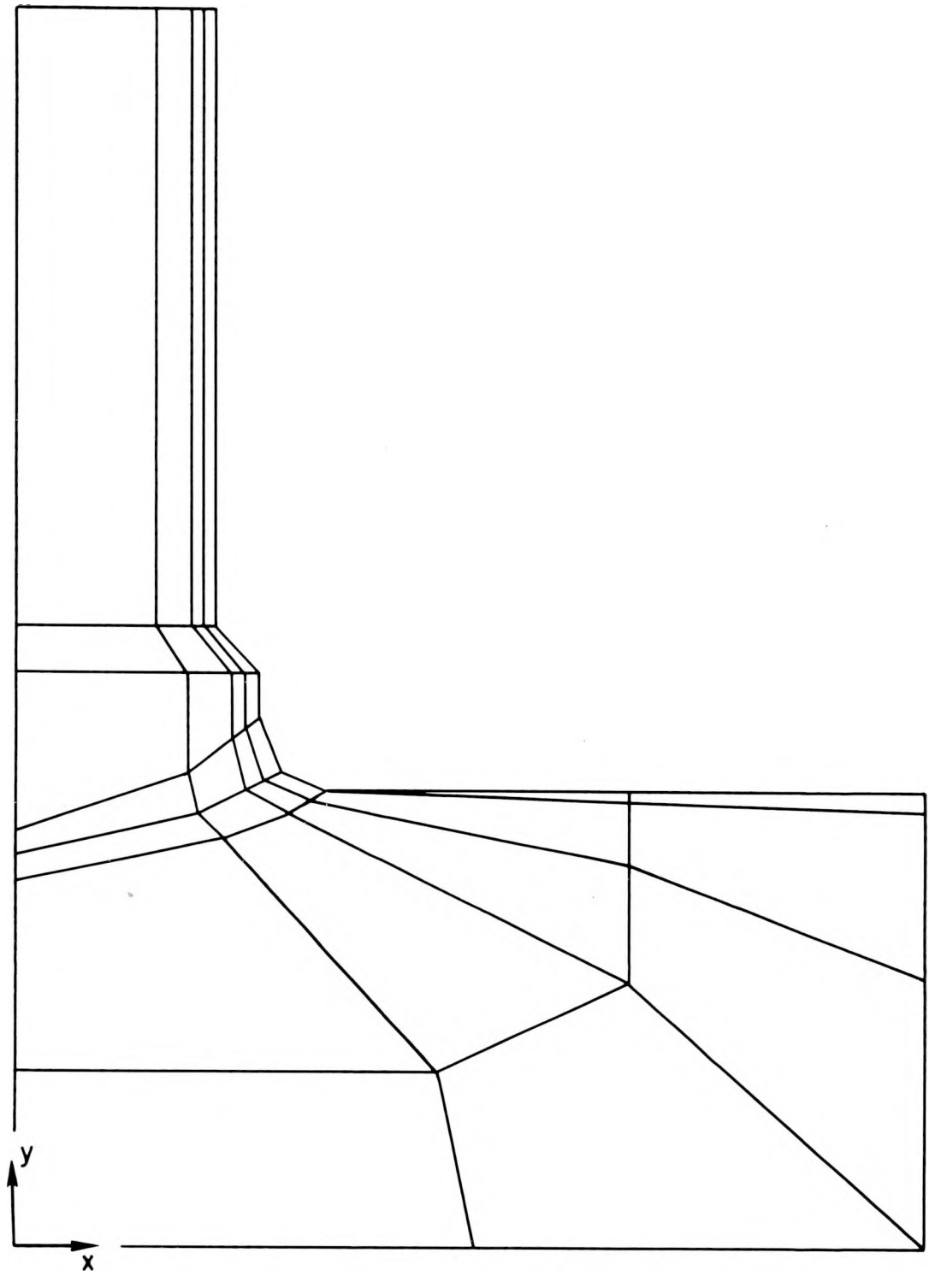

Fig. 2.6. Side view of outside surface of finite-element mesh generated by NOZ-FLAW for ITV configuration.

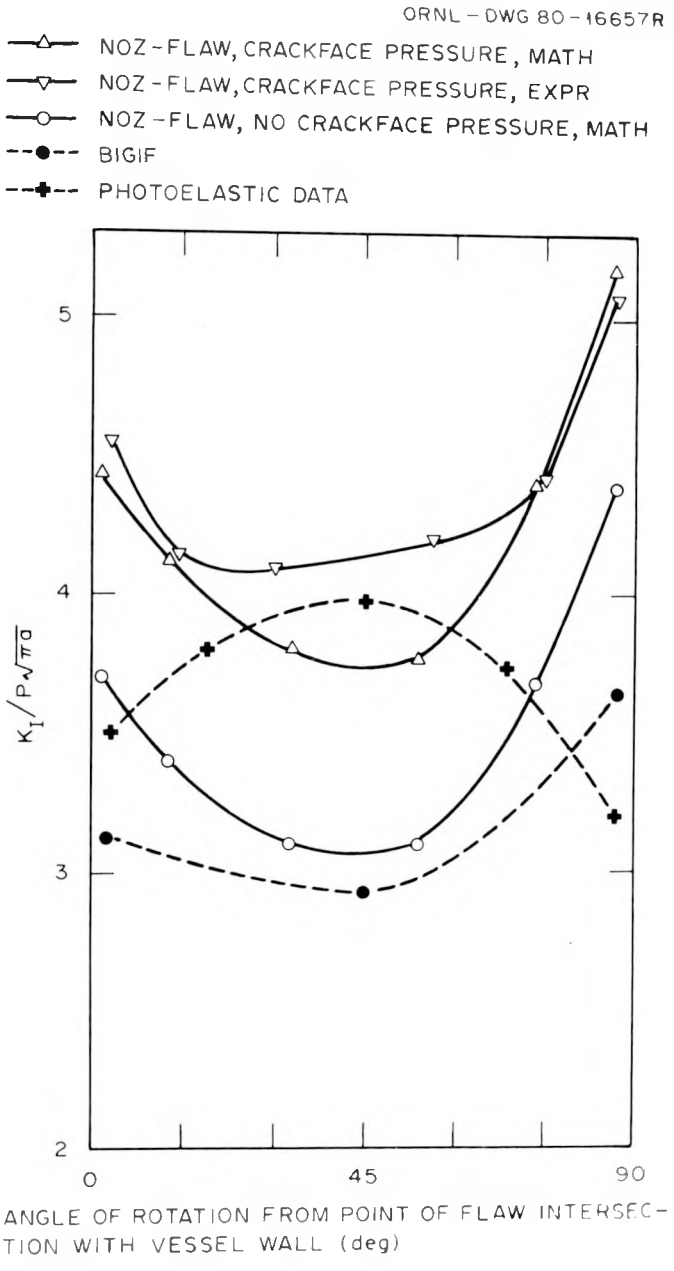

Fig. 2.7. Variation of K_I along a quarter-circular flaw and a natural flaw in an ITV configuration (a/w = 0.41, a = 95 mm).

are presented for the quarter-circular flaw using the BIGIF (Ref. 3) computer program which employs an influence function approach. Note the different trends for K_I that are predicted photoelastically and analytically. Also note that the inclusion of crackface pressure significantly elevates the NOZ-FLAW calculated K-values. Each of the NOZ-FLAW analyses required 1200 K of memory and approximately 28 min of central processing unit (CPU) time on the UCCND IBM 370/3033.

2.2 Investigation of Damping and of Cleavage-Fibrous Transition in Reactor-Grade Steel*

W. L. Fourney†

2.2.1 Introduction

The aim of the research program is to investigate the effect of damping on fracture propagation and to study in detail the transition region between cleavage and ductile fracture. A complete understanding of both of these phenomena is extremely important in predicting fast fracture behavior in a structure.

The program is broken up into four main tasks:

A. Examine the phenomenon of ductile-to-cleavage transition during fracture.

B. Examine closely the effects of damping on the determination of K and on propagation behavior.

C. Conduct dynamic 2-D finite-element computations to support our findings in Tasks A and B.

D. Examine further the effect of higher-order terms on the accuracy of K determinations from photoelastic data so as to permit more accurate damping computations to be made.

Task A is aimed at increasing the understanding of the brittle-to-ductile transition in fracturing. By conducting electron microprobe studies of the fracture surfaces and investigating thickness changes (variations in lateral dimensions) of fractured samples, we hope to develop a plausible model of the stress-strain conditions which control cleavage-fibrous fracturing. The ultimate aim of this Task is to recommend a plan for developing an adequate understanding of the transition region relative to the use of J-R curves and K_{Ic} and K_{Ia} data.

With regard to Task B, we would like to be able to partition the energy loss during fracture into that lost during propagation vs losses that occur after arrest. We are attempting to identify major mechanisms through which losses occur and attribute to them some index of importance which would reveal how much loss could be attributed to each mechanism.

Because fracture energies are proportional to the square of the stress intensity, it is important to know K as accurately as possible. Through Task D, we hope to refine the K values determined photoelastically, so that the minimum amount of computational error is introduced into our damping calculations.

Finite-element computations with the computer code (Task C) are being used to support our findings from both Tasks A and B. In addition, we are using the computer code to predict run-arrest events in thick-walled cylindrical pressure vessels.

---

*Work sponsored by HSST Program under UCCND Subcontract 7778 between Union Carbide Corporation Nuclear Division and the University of Maryland.

†Department of Mechanical Engineering, University of Maryland, College Park, MD 20742.

2.2.2 Progress to date

Task A: Brittle-to-Ductile Transition. As mentioned in the last progress report, we have received to date a number of half samples that were tested either at Del Research Corporation (A 36 steel) or at the Naval Ship Research and Development Center (NSRDC) (A 533 steel). Of the approximately 26 specimens received, we have selected 6 for detailed examinations. We have completed the detailed examination [scanning electron microscope (SEM) and thickness reduction studies] on three of them — two of A 36 steel and one of A 533 steel. The other three specimens selected are being examined, and the results will be available for inclusion in the annual report which will be prepared during the month of October.

Eight specimens still remain to be tested by personnel at NSRDC. Of these, four will probably be tested at 4°C and four above room temperature. Two at each temperature will probably be tested with a spring plate in the loading system and two without the spring plate.

The results of the detailed examinations will be used to develop a preliminary model to describe the cleavage-fibrous transition behavior.

Task B: Damping Studies. Testing required to examine the effects of damping on the run-arrest event has essentially been completed. As reported during the preceding quarter, the effects of artificial ligaments, specimen size, initial crack length, and initial energy level have been determined in plastic specimens. Energy losses caused by specimen vibration, stress wave propagation and modulus change (from static to dynamic and vice versa) have also been investigated. The results of these tests have been analyzed, and a chapter is currently being prepared on the topic for inclusion in the annual report of research results.

Task C: Two-Dimensional Finite-Element Computations. The finite-element code (SAMCR) is being used to predict crack extension behavior in small-sized modified compact tension (MCT) specimens of Homalite 100 (width, $w = 152$ mm) and R_c-46 4340 steel ($w = 104.8$ mm). The reason for using the smaller specimens is to determine the effect of mesh size and mesh density on predicted propagation. The number of elements and nodes used to examine propagation in the regular-sized steel specimens ($w = 209.6$ mm) was at the upper limit of code capability. By taking a specimen one-half the size, it is possible to effectively double the density of the mesh utilized and to determine what effect this will have on predicted propagation. By using the computer code for both Homalite 100 and steel specimens of a smaller size, we hope to separate, to some degree, the material effect from the size effect.

In addition, SAMCR is being used to predict crack jumps in TSE-5 conducted at ORNL. We had reported in the last progress report that static calculations had shown only a 5% difference in predicted stress level at the tip of a crack in a 90° ring segment vs a 180° segment. That calculation was for a short initial crack length. The computation was repeated for a crack with a depth-to-thickness ratio at $a/w = 0.5$, and a 17% difference was found. A full 180° segment is therefore being utilized in the finite-element analysis.

Initial dynamic runs are programmed and ready for submittal for all three crack jump events. The first short jump event has already been run; but, because of an inappropriate choice of K_{Ia} and K_{Ic}, the crack failed

to arrest. We are now in the process of inserting values for K vs a as a function of temperature. Previously, the temperature at the initial length was used to determine only one K vs $\dot{a}$ curve, and this resulted in too low a value for K_{Ia} – thus, the failure to arrest. In the new scheme, the computer will use the temperature at a particular location for the running crack to recall from storage the appropriate K vs $\dot{a}$ curve. This will be used with the K computed at the crack tip to determine if the crack is moving and, if so, the velocity and the propagation during each particular time step.

The results from SAMCR for TSE-5 and the mesh size examinations should both be available for inclusion in the yearly report.

Task D: Higher-Order Terms. The specific aim of this task is to determine the influence of specimen size and geometry on higher-order terms necessary to determine accurately stress intensity factors from photoelastic isochromatic fringe patterns.

The need for these higher-order terms when accurate determinations of K are required has been established previously.[4-6] The principal aim of the work described in this section has been to characterize the behavior of some of the lowest-order nonsingular terms as the crack extends in different fracture test specimens, as well as to formulate and quantify a suitable criterion for the singularity-dominated zone size in these specimens.

Our original intention was to use stress-freezing techniques for growing natural cracks to the desired length in the specimens to be used. Problems encountered with the material being used delayed progress on this task considerably, and we probably will have to undertake casting (in sheet form) of a more suitable material to use the stress-freezing technique satisfactorily. In the meantime, a considerable amount of progress has been achieved using two different sizes of an MCT specimen with saw-cut cracks under static loading. In addition, some work has been completed on evaluating the accuracy of the multiple data point least squares method when applied to photoelastic fracture data.[6,7] The results from both these studies will be summarized and discussed briefly in this section.

Figure 2.8 shows the changes in the isochromatic fringe patterns surrounding a static crack tip as the crack is extended from a/w = 0.5 to a/w = 0.8 in an MCT specimen (w = 203.2 mm). The increased influence of the approaching normal boundary is readily apparent, and features can clearly be discerned in the patterns that require the use of nonsingular terms in the analysis. The circle drawn on each of the photographs is centered on the crack tip and has a radius of 25.4 mm (0.125w), and it represents the boundary of the region from which data points were taken for analysis purposes. A similar series of fringe patterns was recorded in a smaller-sized MCT specimen (w = 102 mm). Figure 2.9 compares the fringe patterns from the larger MCT (LMCT) specimen (w_L = 203 mm) with those from the smaller MCT (SMCT) specimen (w_S = 101.6 mm). Notice that the photographs from the smaller specimen are printed at twice the magnification of the ones for the larger specimen.

Stress field representation in the x, y plane used was based on the Airy Stress Function for a static stress field involving a single crack tip, with the origin located at the crack tip and the negative x-axis

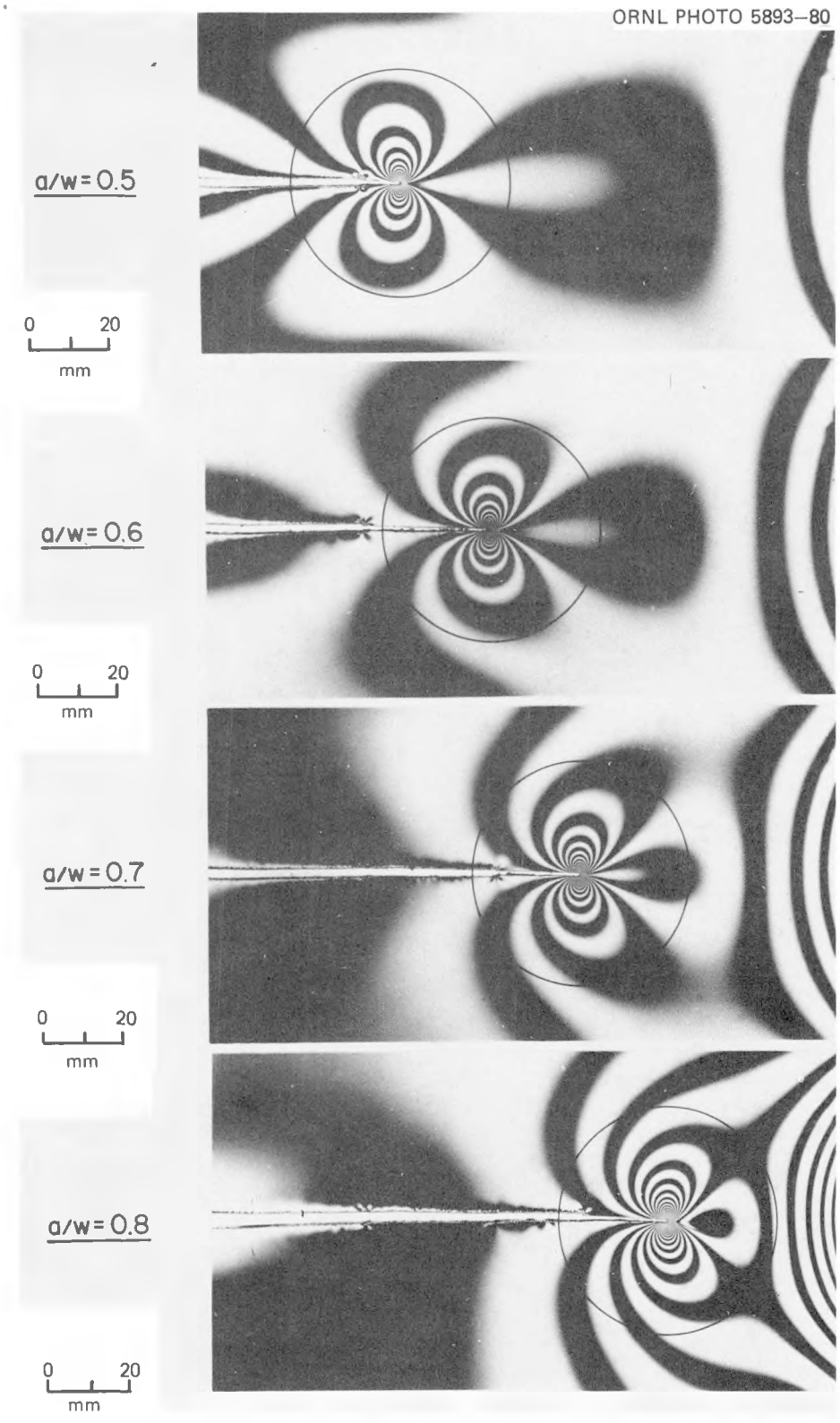

Fig. 2.8. Fringe patterns at four different locations in an MCT specimen illustrating the effect on the fringe pattern of the approaching normal boundary.

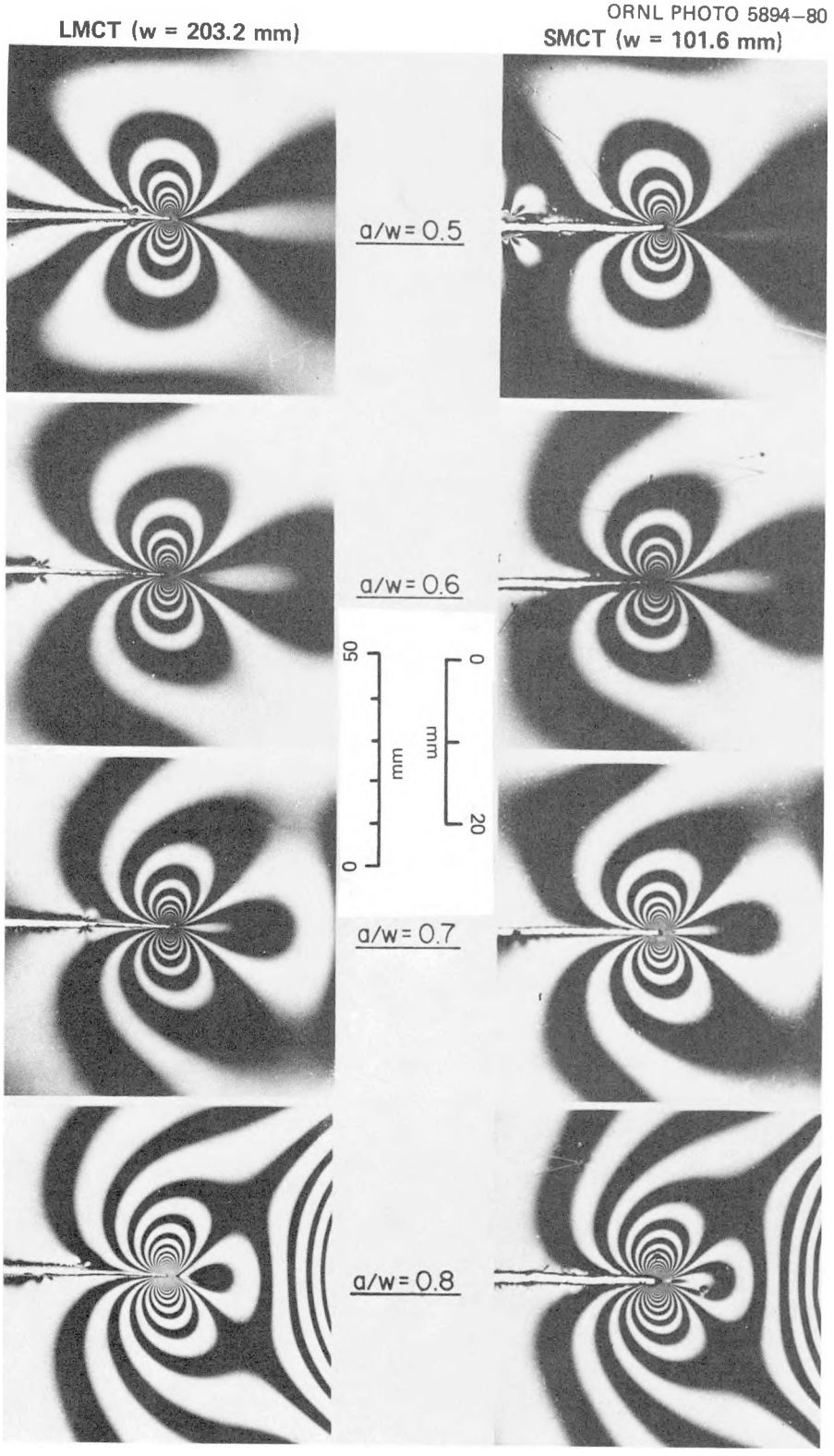

Fig. 2.9. Isochromatic fringe patterns recorded at the same a/w in two different sizes of the MCT specimen.

coinciding with the crack faces. The stress function may then be written as

$$F = \mathrm{Re}\bar{\bar{Z}} + y\ \mathrm{Im}\ (\bar{Z} + \bar{Y}) \ , \tag{1}$$

where

$$Z(z) = \sum_{n=0}^{N} A_n z^{n-(1/2)} \ , \tag{2}$$

$$Y(z) = \sum_{m=0}^{M} B_m z^m \ , \tag{3}$$

$$z = x + iy \ , \tag{4}$$

$$Z = \frac{d\bar{Z}}{dz} \ , \tag{5}$$

$$\bar{Z} = \frac{d\bar{\bar{Z}}}{dz} \ , \tag{6}$$

$$Y = \frac{d\bar{Y}}{dz} \ , \tag{7}$$

and A_n and B_m are real constants. The details of the multiple point least squares method for obtaining the coefficients can be found in Ref. 6 and will not be discussed here.

Analysis using sampled least squares. A question that needed to be addressed was the accuracy with which the least squares method would determine the required coefficients when used with a large number of data points distributed over the region of interest. In addition, obtaining some measure of the variability of the coefficient values computed was felt to be necessary.

A data base was selected for this purpose and consisted of 120 data points from the pattern recorded in the LMCT specimen at a/w = 0.80, taken over the circular region of radius 0.125w shown in Fig. 2.8. One hundred subsets of 30 data points each were selected at random from the data base

and analyzed to obtain the first six stress function coefficients (A_0 to A_2 and B_0 to B_2). As shown in Ref. 6, at least six coefficients are required to adequately characterize the stress field in a region of this size at this location in an MCT specimen.

Results showed that there are two alternative solution sets, one of which has considerably lower fringe order error, $|\Delta n|$. This is illustrated in Fig. 2.10(a and b), which shows $|\Delta n|$ as a function of the computed K-value and the frequency distribution of $|\Delta n|$ respectively. Similar distributions were obtained for all the coefficients, and these are shown in Fig. 2.11. The major points to be noted are

1. the existence of two distributions, one with substantially more data points associated with it (78 vs 22), as well as a lower error and a much narrower spread in the coefficient value, and
2. the fact that these coefficients occur in distinct sets, that is, a particular value of $|\Delta n|$ (large or small) will determine whether the coefficients computed belong to Set 1 or Set 2.

The mean and standard deviation for each of the six coefficients, and for $|\Delta n|$, have been computed by considering the two solution sets separately; the results are listed in Table 2.1. Figure 2.12 shows the experimentally recorded fringe pattern over the data acquisition region and computer plots of the isochromatic fringe patterns predicted by Solution Sets 1 and 2. Experimental and predicted fringe patterns have been shown over the same region and to the same scale for easier comparison. Solution Set 2 clearly provides the "correct" best-fit solution for this particular fringe pattern.

For comparison purposes, three additional solutions were obtained from the complete data base of 120 points. In Trial 1, 60 data points

Table 2.1. Parameter values associated with Solution Sets 1 and 2 from the sampled least squares method

Parameter	Solution Set 1		Solution Set 2		$1 - M_1/M_2$ (%)
	Mean, M_1	Standard deviation	Mean, M_2	Standard deviation	
K ($kPa\cdot\sqrt{m}$)	1711.23	53.55	1868.69	6.63	8.4
B_0 (kPa)	6.48	218.77	1024.56	36.75	99.4
A_1 [$MPa\cdot m^{-(1/2)}$]	18.92	6.60	−37.64	1.37	150.3
B_1 ($MPa\cdot m^{-1}$)	−61.46	6.94	39.61	3.40	255.1
A_2 [$MPa\cdot m^{-(3/2)}$]	459.80	107.06	−373.99	39.29	222.9
B_2 ($MPa\cdot m^{-2}$)	−666.76	275.72	364.96	71.07	282.7
$\overline{\lvert\Delta n\rvert}$	0.2700	0.0492	0.0597	0.0131	−352.3

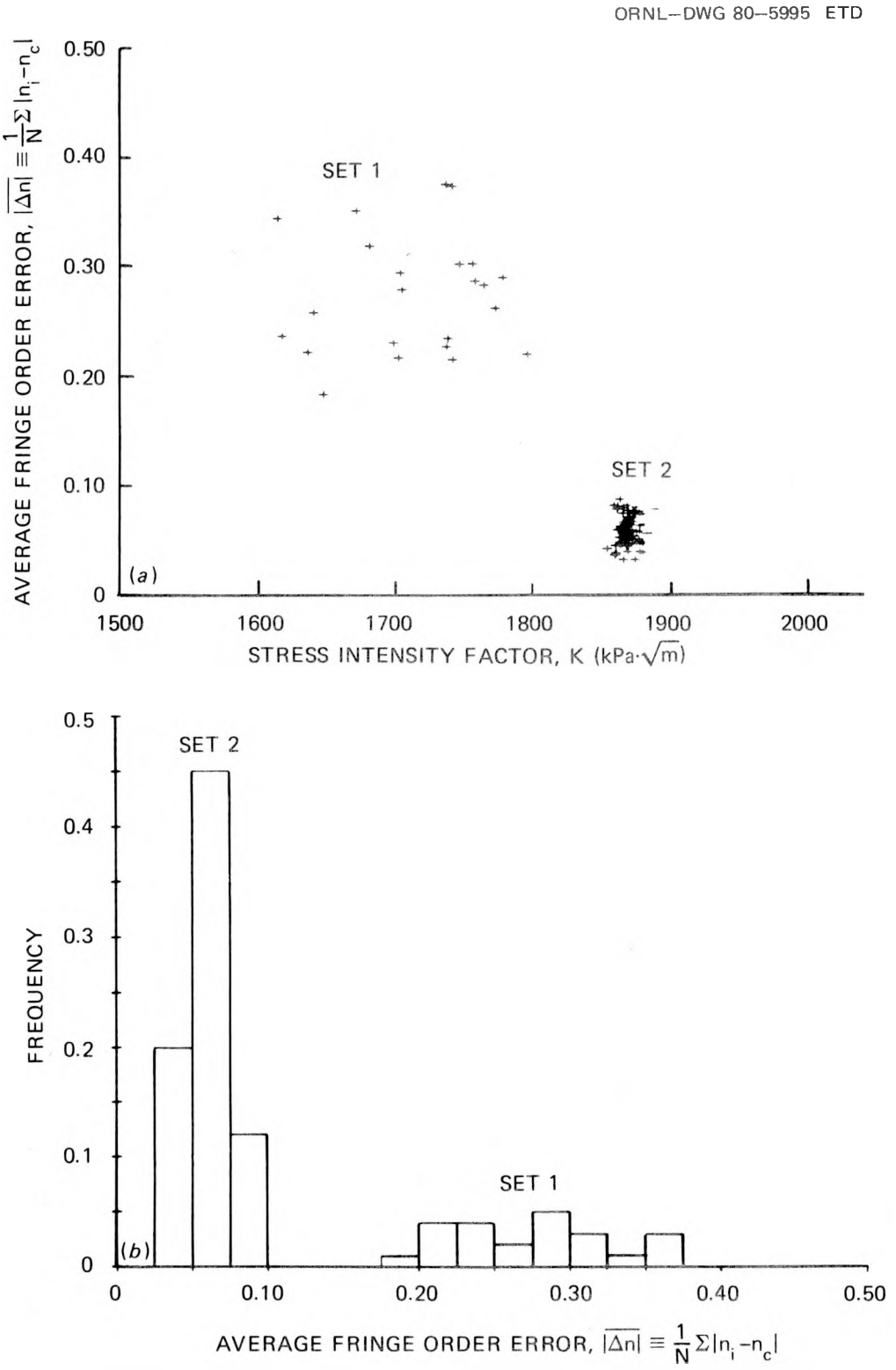

Fig. 2.10. Results from the sampled least squares method showing (a) average fringe order error as a function of the computed K-value and (b) frequency distribution for the average fringe order error.

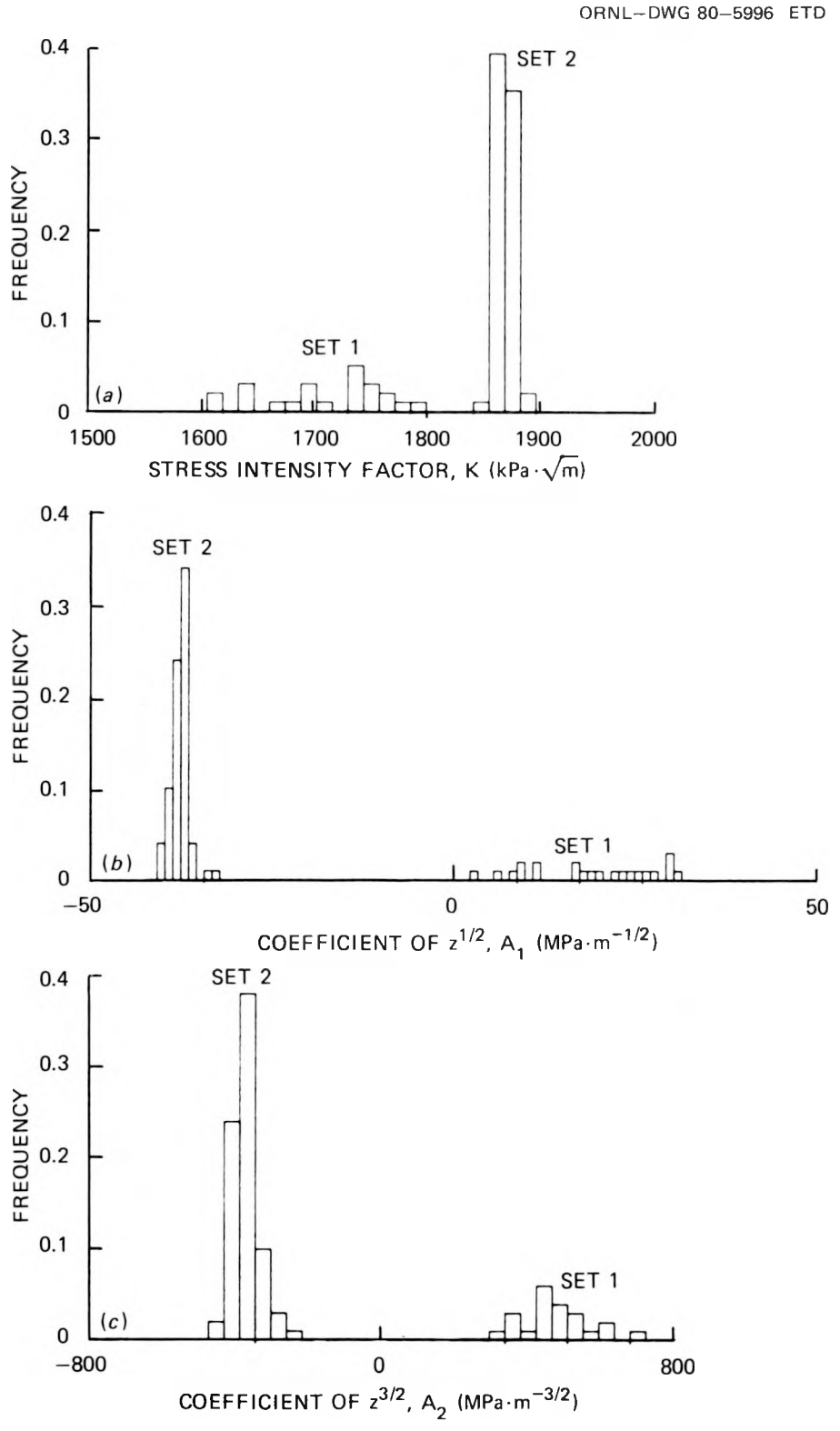

Fig. 2.11. Frequency distribution of the computed values of (a) stress intensity and (b through f) coefficients A_1, A_2, B_0, B_1, and B_2.

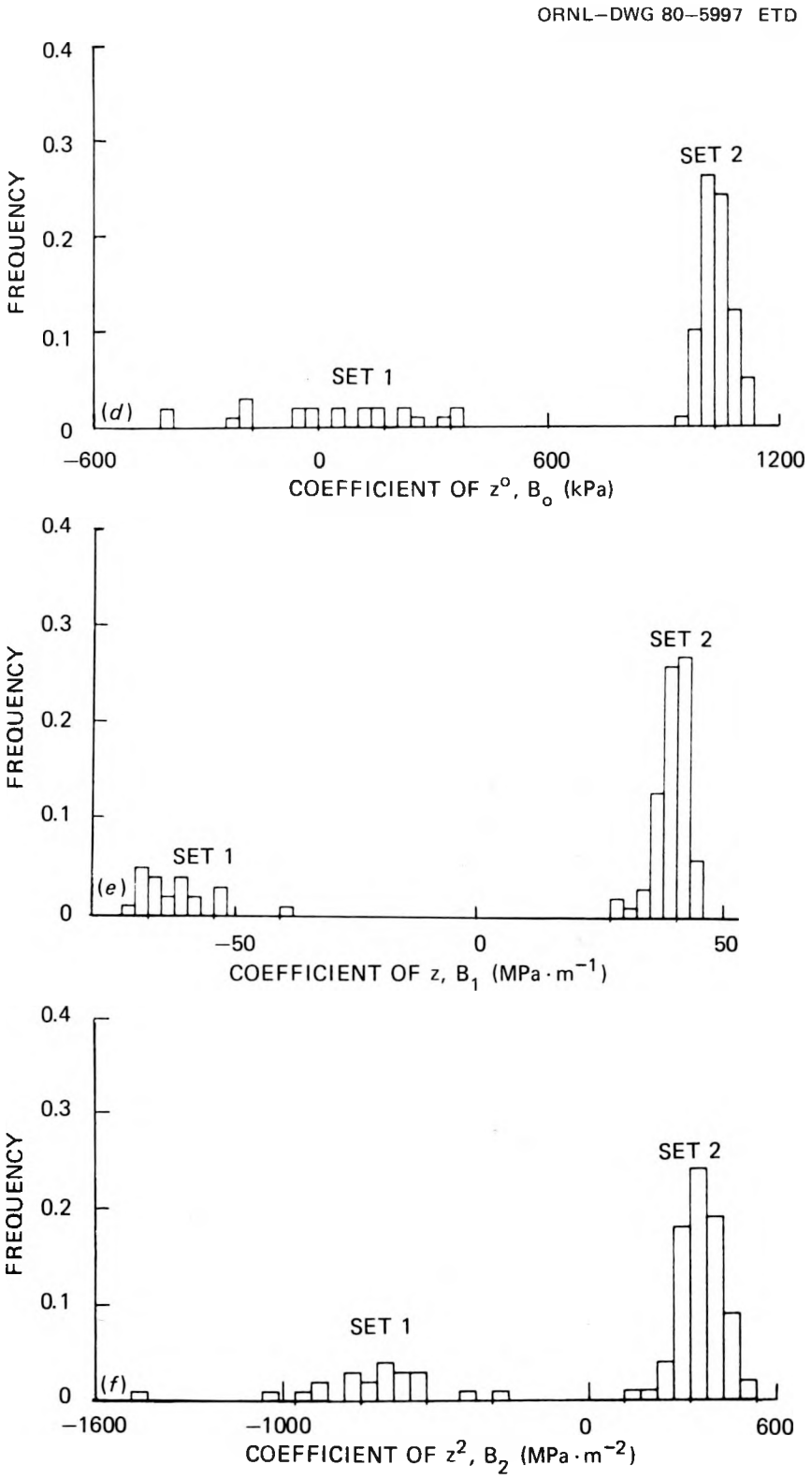

Fig. 2.11 (continued)

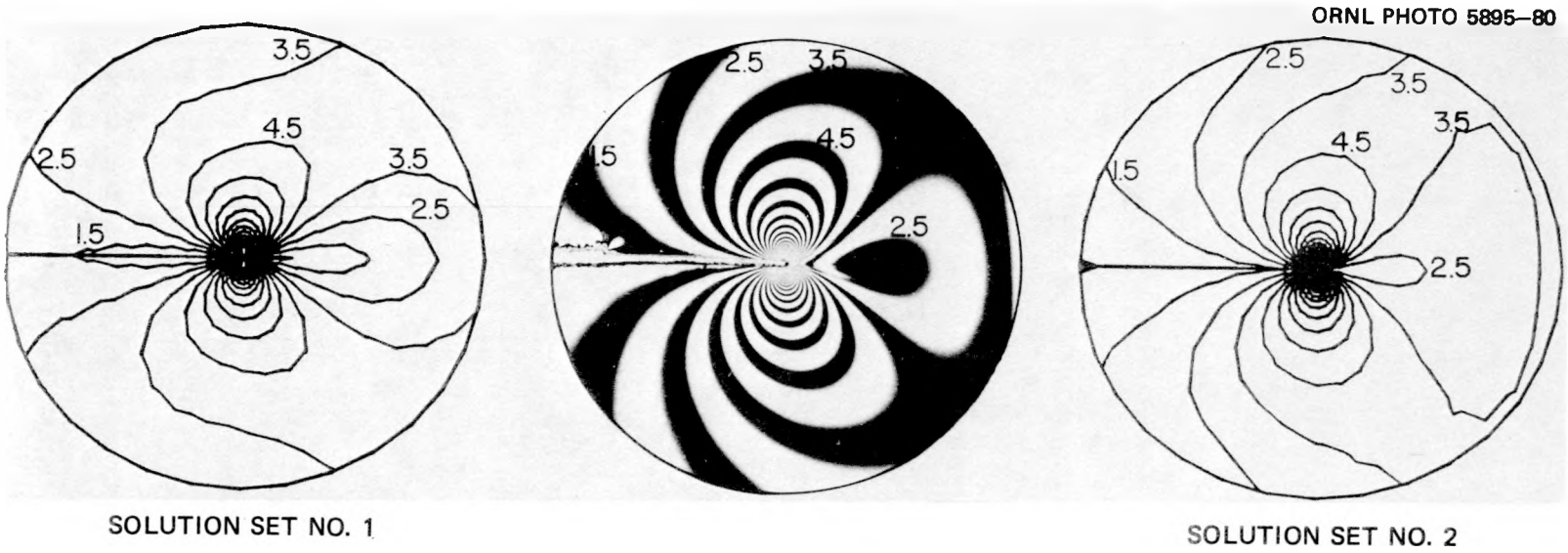

Fig. 2.12. Experimentally recorded isochromatic fringe pattern at a/w = 0.8 in the LMCT specimen and the fringe patterns predicted by solution sets 1 and 2 from the sampled least squares method.

were taken from a region restricted to a maximum radius of 12.7 mm ($r \leq 0.0625w$), while Trial 2 used 60 data points from a region for which the radius was between 12.7 and 25.4 mm ($0.0625w \leq r \leq 0.125w$). Trial 3 used the entire 120 points, which were obtained by combining the data points from Trials 1 and 2. Good agreement was obtained between the coefficients computed from all three trials, as well as the results for Solution Set 2 from the sampling procedure, and these results are summarized in Table 2.2. Figure 2.13 shows the experimental pattern and that predicted by the six-parameter solution from Trial 3; and, once again, good agreement is observed between experimental and predicted fringe patterns.

Table 2.2. Parameter values from whole field data and the sampled least squares method for a/w = 0.80 in the LMCT specimen

Parameter	Trial 1[a] (60 points)	Trial 2[b] (60 points)	Trial 3[c] (120 points)	Solution Set 2
K ($kPa\cdot\sqrt{m}$)	1872.3	1849.4	1868.6	1868.7
B_0 (kPa)	1023.9	1061.8	1028.7	1024.6
A_1 [$MPa\cdot m^{-(1/2)}$]	−38.2	−38.8	−38.3	−37.6
B_1 ($MPa\cdot m^{-1}$)	42.4	41.3	41.7	39.6
A_2 [$MPa\cdot m^{-(3/2)}$]	−443.5	−367.9	−391.4	−374.0
B_2 ($MPa\cdot m^{-2}$)	587.8	340.9	384.7	365.5

[a] 60 data points; $r \leq 0.0625w$.

[b] 60 data points; $0.0625w \leq r \leq 0.125w$.

[c] 120 data points; $r \leq 0.125w$; Data Set 3 = Data Set 1 + Data Set 2.

Results from the SMCT and LMCT specimens. The eight fringe patterns shown in Fig. 2.9 were analyzed using 120 data points taken over a region of radius 0.125w. Figure 2.14 shows the variation in the average fringe order error for each case, as the number of coefficients used was increased. Clearly, the number of parameters necessary for a stable, converging solution increases sharply as the crack tip approaches a normal boundary. The ability of a six-parameter solution to accurately predict the fringe pattern at a/w = 0.80 in the LMCT specimen has already been demonstrated. A similar comparison of experimental and predicted fringe patterns for the SMCT specimen at a/w = 0.80 is shown as Fig. 2.15.

The results obtained for the different crack lengths in the SMCT and LMCT specimens are summarized in Table 2.3. The power law in terms of the specimen width w that is used to cast the coefficients in a convenient specimen-size-independent dimensionless form comes from rewriting Eqs. (2)

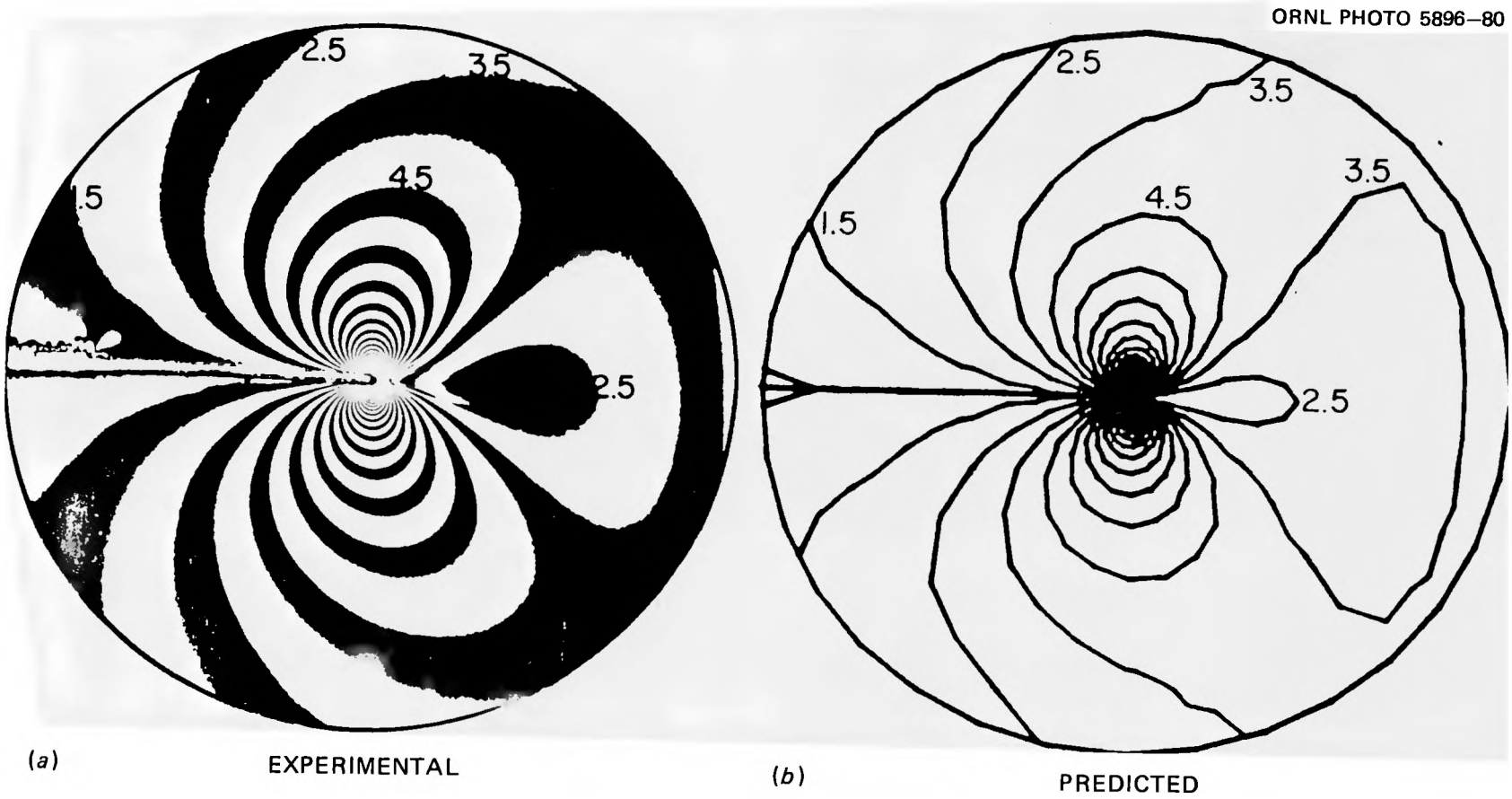

Fig. 2.13. Experimental and predicted fringe patterns at a/w = 0.8 in the LMCT specimen.

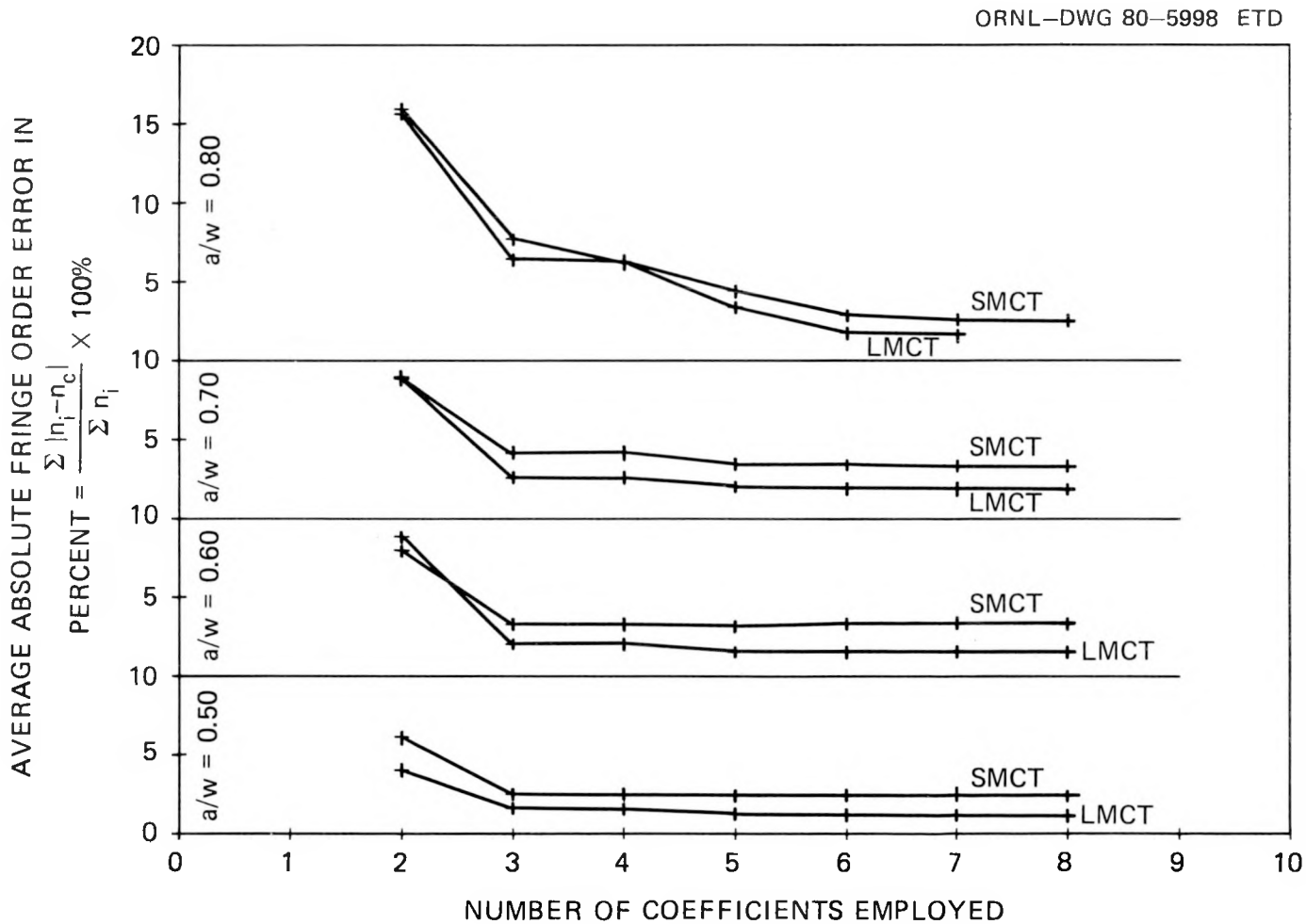

Fig. 2.14. Average absolute fringe order error as a percentage of average input fringe order shown as a function of number of coefficients employed in the stress field representation.

ORNL PHOTO 5897–80

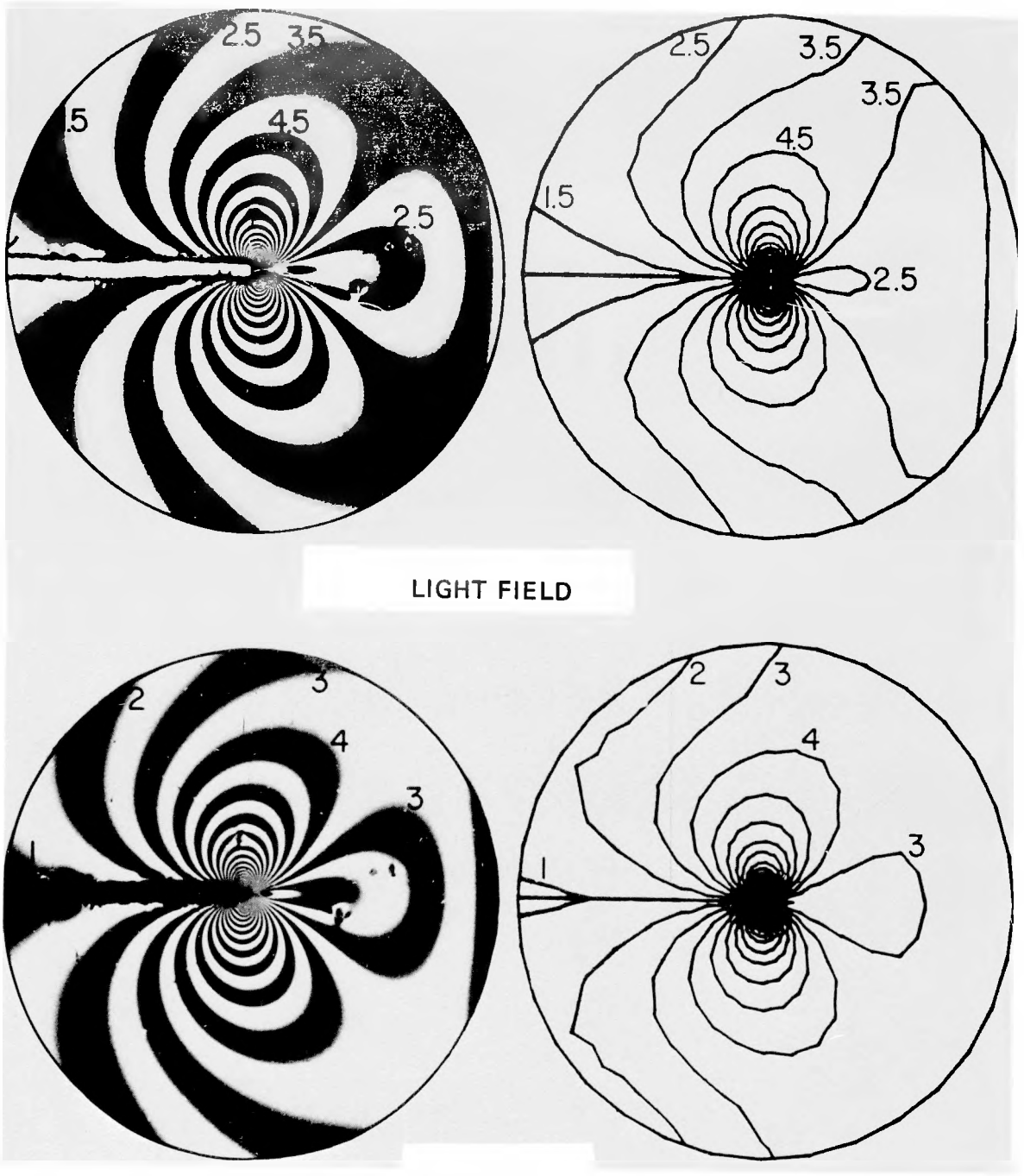

Fig. 2.15. Experimental and predicted fringe patterns at a/w = 0.8 in the SMCT specimen.

Table 2.3. Coefficient ratios from a seven-parameter solution for different crack lengths in SMCT and LMCT specimens

a/w	Coefficient ratio	z^b	Coefficient ratio from SMCT (w_S = 101.6 mm)	Coefficient ratio from LMCT (w_L = 203.2 mm)	SMCT/LMCT	$(w_L/w_S)^b$
0.50	B_0/A_0	$z^{1/2}$	0.3086	0.1702	1.813	1.414
	A_1/A_0	z^1	−0.9411	−0.4864	1.935	2.000
0.60	B_0/A_0	$z^{1/2}$	0.3147	0.1656	1.900	1.414
	A_1/A_0	z^1	−1.2140	−0.5929	2.048	2.000
	B_1/A_0	$z^{3/2}$	0.1265	0.0583	2.170	2.828
0.70	B_0/A_0	$z^{1/2}$	0.2383	0.1913	1.246	1.414
	A_1/A_0	z^1	−1.3322	−0.7396	1.801	2.000
	B_1/A_0	$z^{3/2}$	0.2143	0.0661	3.242	2.828
0.80	B_0/A_0	$z^{1/2}$	0.3283	0.2177	1.508	1.414
	A_1/A_0	z^1	−2.2324	−1.2698	1.758	2.000
	B_1/A_0	$z^{3/2}$	0.4675	0.2087	2.240	2.828
	A_2/A_0	z^2	−1.2895	−0.3375	3.821	4.000
	B_2/A_0	$z^{5/2}$	0.4894	0.0704	6.952	5.657

and (3) as follows

$$Z(z) = A_0 z^{-(1/2)} \sum_{n=0}^{N} \frac{A_n}{A_0} z^n$$

$$= A_0 z^{-(1/2)} \sum_{n=0}^{N} \frac{A_n}{A_0} w^n \left(\frac{z}{w}\right)^n$$

$$= A_0 z^{-(1/2)} \sum_{n=0}^{N} A'_n \left(\frac{z}{w}\right)^n , \tag{8}$$

and

$$Y(z) = A_0 z^{-(1/2)} \sum_{m=0}^{M} \frac{B_m}{A_0} z^{m+(1/2)}$$

$$= A_0 z^{-(1/2)} \sum_{m=0}^{M} \frac{B_m}{A_0} w^{m+(1/2)} \left(\frac{z}{w}\right)^{m+(1/2)}$$

$$= A_0 z^{-(1/2)} \sum_{m=0}^{M} B'_m \left(\frac{z}{w}\right)^{m+(1/2)} . \tag{9}$$

Figure 2.16 shows the experimentally obtained coefficient ratio, (SMCT/LMCT), vs the theoretical ratio of the w-values raised to the appropriate power, $(w_L/w_S)^b$, b = 1/2, 1, 3/2, etc.

Table 2.4 shows the values of the first three nonsingular terms, B_0, A_1, and B_1, in their normalized form. The normalized coefficients have been plotted as functions of a/w in Fig. 2.17 with smooth curves drawn

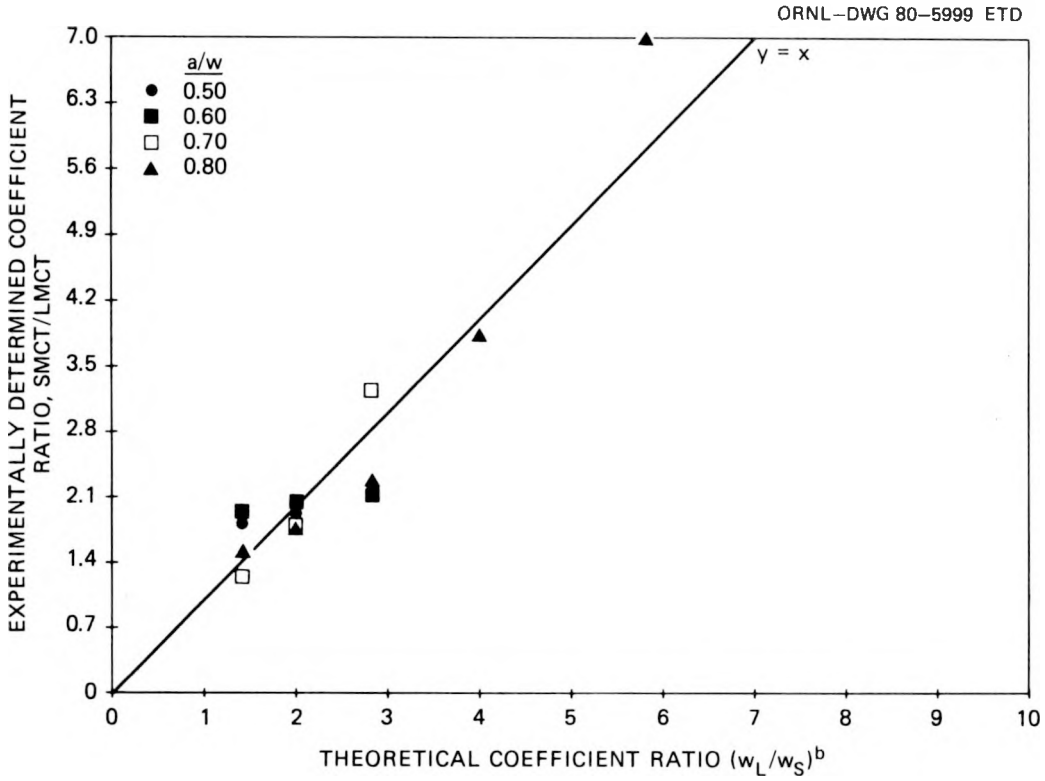

Fig. 2.16. Experimentally determined coefficient ratio vs theoretical prediction.

Table 2.4. Normalized forms of the three lowest-order nonsingular terms in a modified compact tension specimen

Nonsingular term	Specimen	a/w = 0.50	a/w = 0.60	a/w = 0.70	a/w = 0.80
$B_0' = \frac{B_0}{A_0} w^{1/2}$	SMCT	0.6173	0.6293	0.4765	0.6567
	LMCT	0.4815	0.4684	0.5411	0.6157
	Mean	0.5494	0.5489	0.5088	0.6362
$A_1' = \frac{A_1}{A_0} w^1$	SMCT	−3.765	−4.857	−5.329	−9.297
	LMCT	−3.721	−4.744	−5.917	−10.159
	Mean	−3.743	−4.800	−5.623	−9.728
$B_1' = \frac{B_1}{A_0} w^{3/2}$	SMCT	1.5280	1.0120	1.7140	3.7401
	LMCT	0.9690	1.3190	1.4960	4.7223
	Mean	1.2470	1.1660	1.6050	4.2311

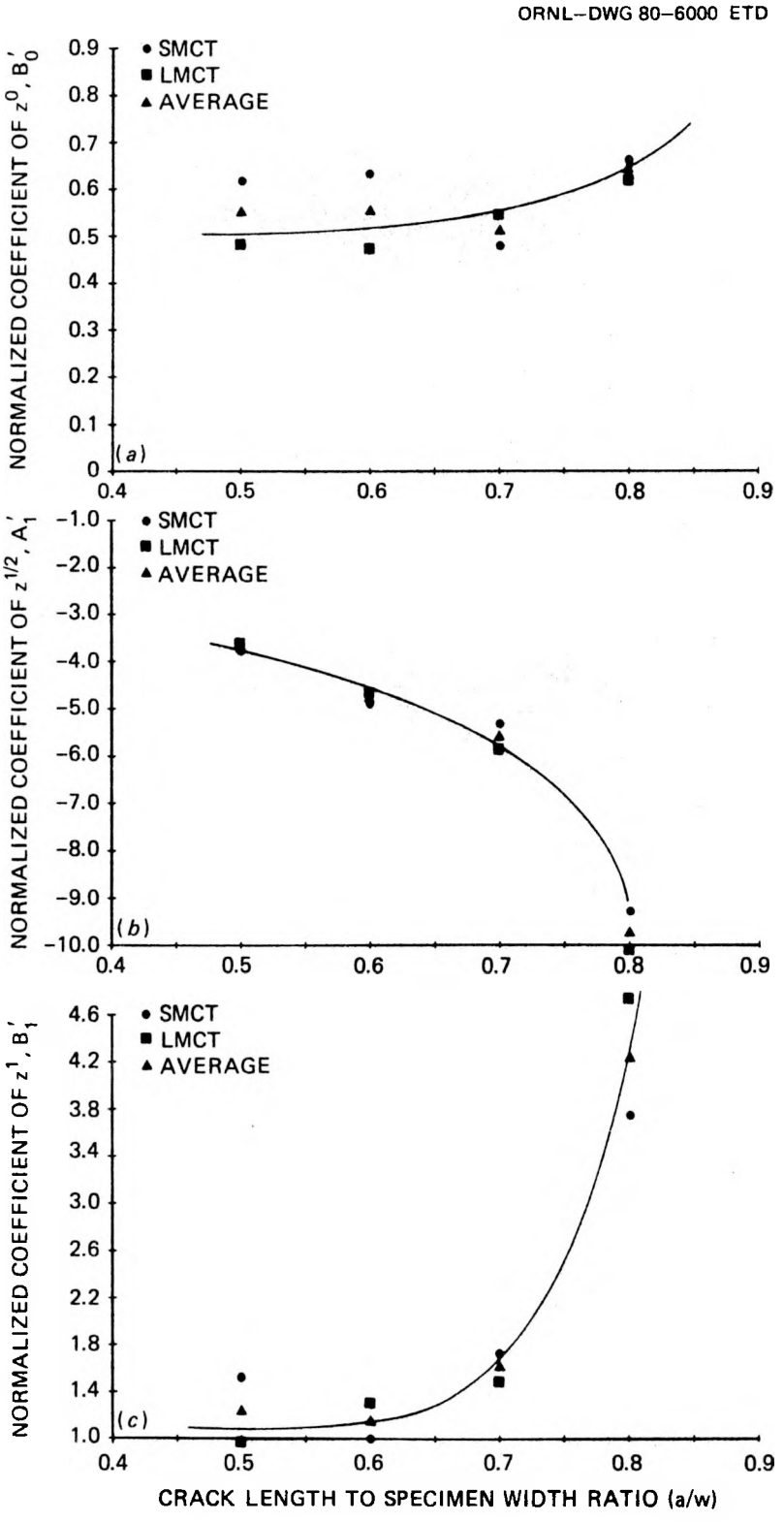

Fig. 2.17. Variation with a/w in the MCT specimen of the normalized coefficients of (a) z^0, (b) $z^{1/2}$, and (c) z^1.

through the data points. These curves are only meant to show the trend exhibited by these nonsingular terms, and more data will be needed before a set of standard reference curves can be generated.

To complete this first phase of the study, our intention is to obtain some additional data for the MCT specimen and to complete a similar study using a standard-sized wedge-loaded rectangular double cantilever beam (RDCB) specimen. Complete stress field representations obtained in this manner for the MCT and RDCB specimens will then be used to obtain estimates of the singularity-dominated zone size in the two specimens.

References

1. B. R. Bass, J. W. Bryson, and K. Kathiresan, *NOZ-FLAW: A Finite-Element Program for Direct Evaluation of Stress Intensity Factors for Pressure Vessel Nozzle-Corner Flaws*, ORNL/NUREG/CSD/TM-18, Oak Ridge National Laboratory (to be published).

2. C. W. Smith, M. Jolles, and W. H. Peters, *Stress Intensities for Nozzle Cracks in Reactor Vessels*, VPI-E-76-25, ORNL/Sub-7015/1, Virginia Polytechnic Institute and State University (November 1976).

3. P. M. Besuner, D. C. Peters, and R. C. Cipolla, *BIGIF: Fracture Mechanics Code for Structures*, NP-838, Failure Analysis Associates (July 1978).

4. R. J. Sanford, "A Critical Re-examination of the Westergaard Method for Solving Opening-Mode Crack Problems," *Mechanics Research Communications* 6, 289–94 (1979).

5. R. Chona, G. R. Irwin, and A. Shukla, "A Comparison of Two and Three Parameter Representations of the Stress Field Around Static and Dynamic Cracks," *Experimental Mechanics* (to appear).

6. G. R. Irwin et al., *Photoelastic Studies of Damping, Crack Propagation, and Crack Arrest in Polymers and 4340 Steel*, U.S. NRC Report NUREG/CR-1455, Washington, D.C. (1979).

7. R. J. Sanford, "Application of the Least Squares Method to Photoelastic Analysis," *Experimental Mechanics* 20, 192–7 (1980).

3. INVESTIGATIONS OF IRRADIATED MATERIALS*

3.1 Third 4T-CTS Irradiation Study

D. A. Canonico T. N. Jones
R. G. Berggren

Approximately 30% of the irradiated Charpy V-notch (C_V) impact specimens from this irradiation experiment were tested in the initial test series, and the results were reported in a previous quarterly report.[1] We are preparing to complete Charpy impact testing of specimens from this irradiation experiment, thereby providing additional data on "upper-shelf energy" as a function of fast neutron fluence and irradiation temperature. We are reinstalling the tensile test equipment in a hot cell to test the tensile test specimens from this experiment.

3.2 Fourth HSST Irradiation Series

J. W. Woods R. G. Berggren
T. N. Jones D. A. Canonico

Irradiation of the first capsule, capsule A, of this irradiation series[2] continued through this quarter. Accumulated exposure for the capsule through Sept. 30, 1980, is 4423 h. Temperature control continued to be excellent with variations near those previously reported.[1] We expect to remove this capsule from the reactor in October 1980, at which time the specimens will have been irradiated to the desired fluence of 2×10^{19} neutrons/cm^2, E > 1 MeV.

Irradiation of the second capsule, capsule B, of this series was initiated on June 26, 1980. Accumulated exposure for this capsule as of Sept. 30, 1980, is 1456 h. Temperature control is good but not quite as good as for the first capsule of this series. The average temperature (average for 39 thermocouples) is 286°C. Two of the thermocouples at the top corners of the specimen array are reading about 11 K below average and the remaining thermocouples are reading within 7 K of the average temperature.

Parts are on order for the third capsule of this series, and final specimen preparation is in progress.

Parts are on order for the fourth capsule of this series, and specimens are being prepared by Materialprufungsanstalt (MPA), Stuttgart, Germany.

---

*Conversions from SI to English units for all SI quantities are listed on a foldout page at the end of this report.

References

1. D. A. Canonico et al., "Investigation of Irradiated Materials," *Heavy-Section Steel Technology Program Quart. Prog. Rep. April–June 1980*, NUREG/CR-1627 (ORNL/NUREG/TM-401), pp. 18–27.

2. R. G. Berggren et al., "Investigations of Irradiated Materials," *Heavy-Section Steel Technology Program Quart. Prog. Rep. July–September 1979*, ORNL/NUREG/TM-370, pp. 27–39.

4. THERMAL SHOCK INVESTIGATIONS*

R. D. Cheverton S. E. Bolt
S. K. Iskander P. P. Holz

During this report period for the Thermal Shock Program, a heat transfer experiment was conducted with the TSE-5A test cylinder (TSC-2), the initial flaw was prepared in TSC-2, TSC-2 was tempered, material characterization studies pertaining to TSC-2 were completed, additional inner-surface coating development studies were conducted, the inner surface of TSC-2 was sprayed in preparation for TSE-5A, and TSE-5A was conducted.

4.1 Heat-Transfer Experiment (TSH-5A-1) Conducted with TSC-2

Prior to TSE-5, two full-scale heat-transfer experiments were conducted with the TSE-5 test cylinder (TSC-1). The results of these experiments[1] and TSE-5[2] indicated that satisfactory thermal shocks could be achieved in the Liquid-Nitrogen Thermal Shock Test Facility. However, a somewhat different inner-surface coating material and application technique were proposed for TSE-5A,[3] and TSE-5A required a more severe thermal shock than that achieved during TSE-5; thus, at least one additional full-scale heat-transfer experiment was necessary prior to TSE-5A.

The "rubber-cement" coating for TSH-5A-1 was applied in six applications. The coating material for the first coat was 3M-34, and for the remaining five coats it was 3M-NF34. The final surface density of the coating was 240 g/m^2. For TSE-5 the surface density was 350 g/m^2. Both of these surface densities are well beyond the optimum coating thickness in terms of maximum quench rate. Provided that the volume density and nucleation-site surface density were the same for the two cases, the thinner coating should have resulted in a more rapid quench rate. As shown in Fig. 4.1, the quench rate for TSH-5A-1 was more rapid for the first 2 min but thereafter was less rapid than that for TSE-5. This behavior indicated that the nucleation-site density for TSH-5A-1 was less than that for TSE-5.

A pretest fracture-mechanics analysis of TSE-5A, based on the TSH-5A-1 thermal transient, indicated that the TSH-5A-1 transient would be only marginally acceptable for a successful TSE-5A experiment. Thus, a higher surface density of nucleation sites on the surface coating for TSE-5A was desirable.

Temperature distributions through the wall of test cylinder TSC-1 and TSC-2 were measured at 15 different locations[2] with 12 thermocouples distributed through the wall at each location. Each set of 12 thermocouples was incorporated in a thimble that was plugged into a snug-fitting hole in the wall at each of the 15 locations. For tests previous to TSH-5A-1,

*Conversions from SI to English units for all SI quantities are listed on a foldout page at the end of this report.

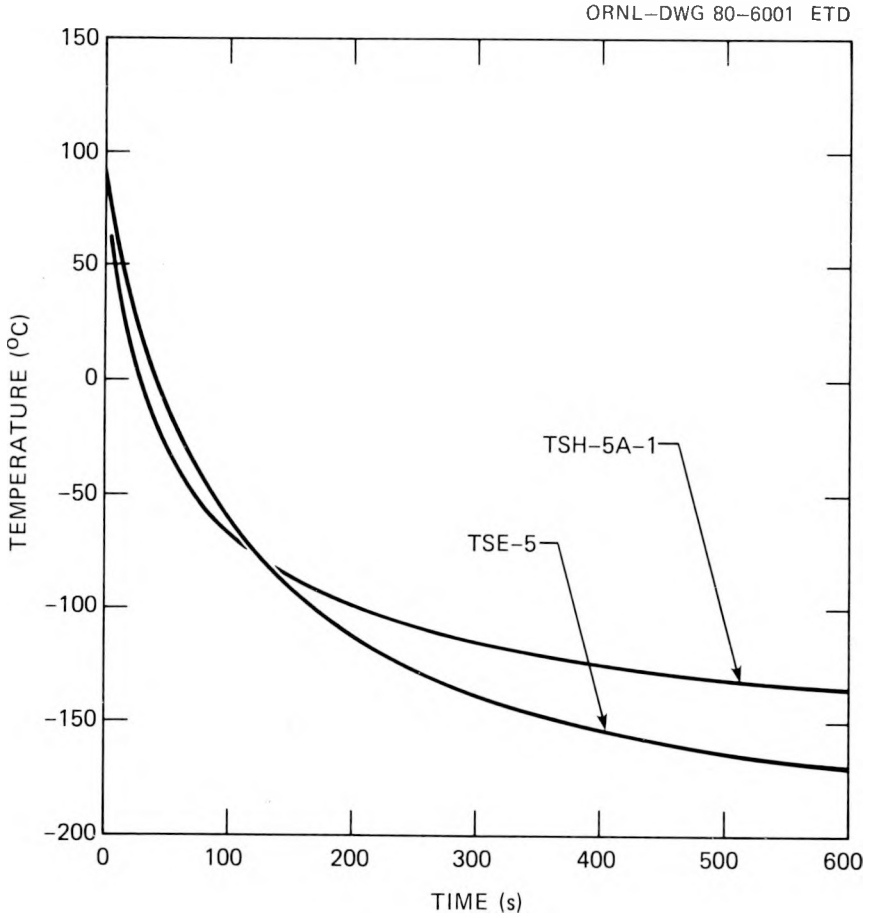

Fig. 4.1. Comparison of inner-surface (a/w = 0.0083) quench rates for TSE-5 and TSH-5A-1.

all of the 15 thimbles were cylindrical with a diameter of 25 mm (see Fig. 4.2). This thimble geometry introduces an error in transient temperature measurements if there is appreciable thermal resistance between the thimble and thimble cavity because the surface of a thimble does not coincide with radial lines (lines normal to the isotherms). If the thermal resistance at the thimble surface were infinite, the error in temperature measurement could be significant for later times in the transient. The actual thermal resistance was expected to be reasonably low. Furthermore, the most interesting part of the transient was the early part, during which time the error in temperature measurement would be small even with infinite resistance. However, the secondary cracking that occurred "late" in the TSE-5 transient created interest in the accuracy of temperature measurements later in the transient. For this reason three tapered rectangular thimbles, as shown in Fig. 4.3, were included in TSC-2 at midlength of the cylinder (all surfaces of these thimbles coincided with radial lines). During TSH-5A-1, there were no consistent significant differences in temperature measurements between the cylindrical and rectangular thimbles, indicating that the surface thermal resistance for the thimbles was negligible.

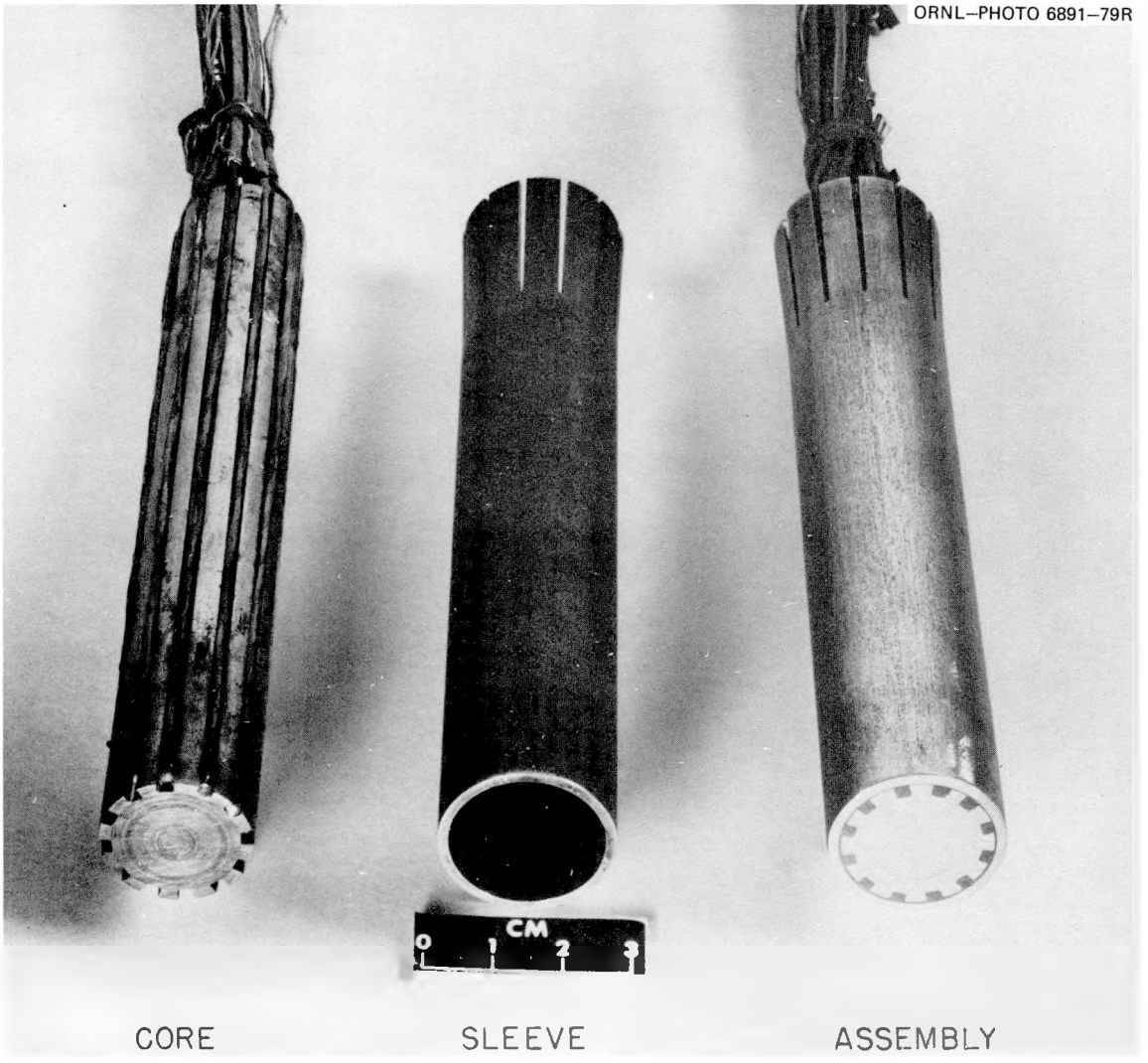

Fig. 4.2. Thermocouple thimble components and assembly for measuring radial temperature distribution in TSC-2 during thermal shock experiments.

A comparison of temperatures at the same radial location for all thimbles indicates the degree of asymmetry in quenching during the transient. During TSH-5A-1, the maximum variation in indicated inner-surface temperatures among the 15 thimbles was 15 K. The trend from one thimble to another was the same for all thermocouples in a thimble, and the variation could not be traced to instrumentation such as the reference junction boxes and data system which are a part of the temperature-measuring system. Thus, there appears to be a real variation in heat transfer rate over the inner surface of the test cylinder. Although there is a certain degree of randomness about the distribution, indicating local random variations in the inner-surface coating, there are nonetheless indications that the upper end of the test cylinder cooled more rapidly than the lower end and that there was an azimuthal variation. The maximum value of the latter variation was ~6 K, and the maximum axial variation was ~8 K.

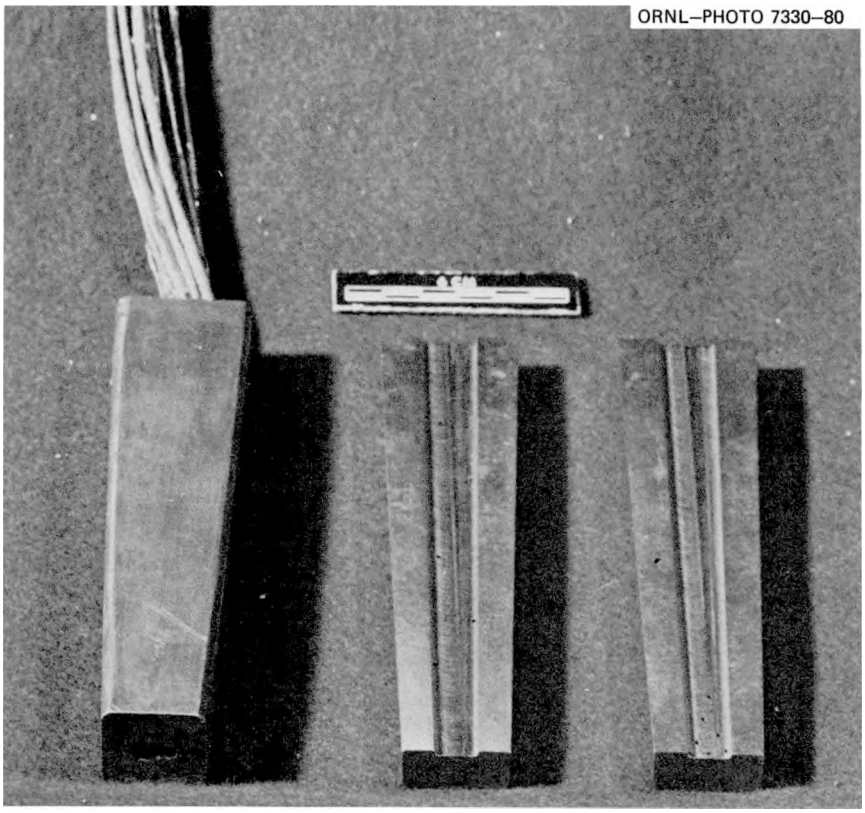

Fig. 4.3. Tapered thermocouple thimble components and assembly for measuring radial temperature distribution in TSC-2 during thermal shock experiments.

These variations, when coupled with the generally random distribution over the inner surface, are negligible in terms of crack behavior and analysis thereof. The same was found to be true for TSE-5.

4.2 Tempering of TSC-2

As discussed in Ref. 3, a tempering temperature of 679 ± 3°C was selected for the TSE-5A test cylinder (TSC-2), and a tempering time of 4 h at this temperature was specified. The unusually close tolerance on temperature was specified because of the sensitivity of fracture toughness to tempering temperature and because the success of TSE-5A depended to some extent on achieving the desired toughness curve with considerable accuracy.

While tempering the TSC-2 prolongation at the same temperature,[3] the greatest variation in temperature during tempering was found to be the variation from top to bottom of the cylinder rather than the timewise variation at a single thermocouple location or that caused by inaccuracies in instrumentation and thermocouple calibration. Thus, a way was devised to effectively insulate the ends of the test cylinder during tempering so as to minimize the axial gradient.

Ten thermocouples, calibrated at 661°C (molten aluminum), were used to map the temperature distribution in TSC-2 during tempering. During the 4-h tempering period, the space-averaged temperature at midlength of the cylinder was 679 ± 1°C, and the space variation at midlength was ±3 K. The temperature at the top of the cylinder was 5 K higher and at the bottom was 5 K lower than that at midlength. The heating time required to arrive at the desired tempering temperature was 7 h. After soaking for 4 h at the tempering temperature, TSC-2 was removed from the furnace and allowed to cool in air with natural convection on the outer and inner surfaces.

4.3 Preparation of Long Axial Flaw for TSE-5A

P. P. Holz

The initial flaws used for thermal shock experiments TSE-1 through TSE-5 were prepared by means of the electron beam (EB) welding technique,[4] and the same general technique was to be used for TSE-5A. For all but TSE-2 the intended initial flaw was an axially oriented sharp crack extending the full length of the test cylinder. However, the EB-weld technique introduces the possibility of short circumferential cracks (cross cracks) because cracking of the EB-weld fusion zone is a result of residual stresses that develop as the fusion zone cools, and these stresses can exist in both the axial and circumferential directions. Cross cracks were not observed in the first four experiments, but they were observed in the EB-weld fusion zone used for TSE-5. One of these cross cracks, which initially were confined to the fusion zone, propagated during TSE-5, causing extensive cracking all over the inner surface of the test cylinder, and as a result complicated the posttest analysis of TSE-5. Thus, additional EB-weld-flawing development studies were conducted prior to preparation of the long axial flaw for TSE-5A in an effort to prevent cross cracking.

As discussed in Refs. 2 and 4, the hydrogen-charging time for post-TSE-5 test welds was much less than that for the TSE-5 weld (4 h compared with ~80 h), and no cross cracking was found in the test welds. Furthermore, as mentioned above, there were no cross cracks when no hydrogen charging was not required. Thus, reducing the charging time would apparently reduce and even eliminate cross cracking.

One possible way of reducing charging time is to contaminate the EB weld. As reported in Ref. 3, an attempt was made to do this by adding an iron-sulfur compound to the weld during the welding process. The initial attempts to do this were not successful, and the effort was abandoned in favor of another approach to reducing cross cracking.

More recent efforts were focused on determining whether weld depth, as controlled by focal current alone, would have an effect on cross cracking. Figure 4.4 contains the results of such a study and shows (1) that weld depth increases with focal current up to ~520 mA and then decreases and (2) that there is no cross cracking up to ~505 mA. The crack depth corresponding to the latter current is ~14 mm, and a crack depth as shallow as 10 mm was considered acceptable for TSE-5A (for TSE-5 the weld depth was 15 mm). Thus, it appeared that cross cracking could be eliminated for TSE-5A.

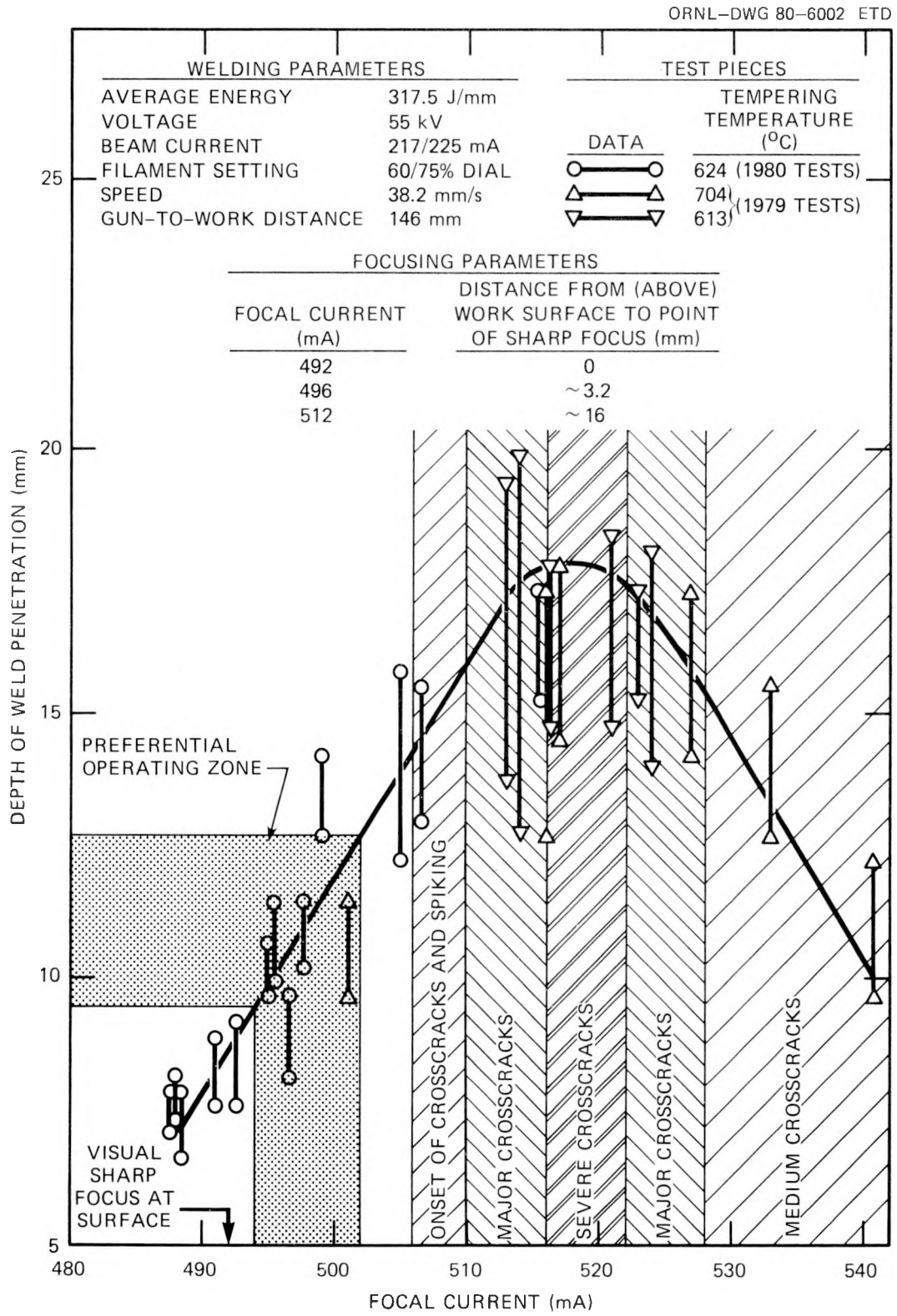

Fig. 4.4. Weld penetration vs focal current in flawing trials with Y-12 Sciaky welder. Test pieces were A508 forging material tempered at 613, 624, and 704°C.

For TSE-5A the values of the various EB-weld parameters were those shown in Fig. 4.4, and the focal current selected was 500 mA. The required hydrogen charging time was 15 h, following hydrogen charging, no cross cracks were observed.

4.4 Materials-Characterization Studies Pertaining to TSE-5A

As discussed in Ref. 3, a tempering temperature of 679°C was selected for TSC-2 on the basis of materials-characterization studies that included fracture-toughness data for three test temperatures and two tempering temperatures including 679°C. Since that time, fracture-toughness data have been obtained for two more testing temperatures for material tempered at 679°C. Furthermore, six values of crack arrest toughness have been determined. The complete set of data for the latter tempering temperature is shown in Fig. 4.5. The K_{Ic} and K_{Ia} curves shown in the figure represent

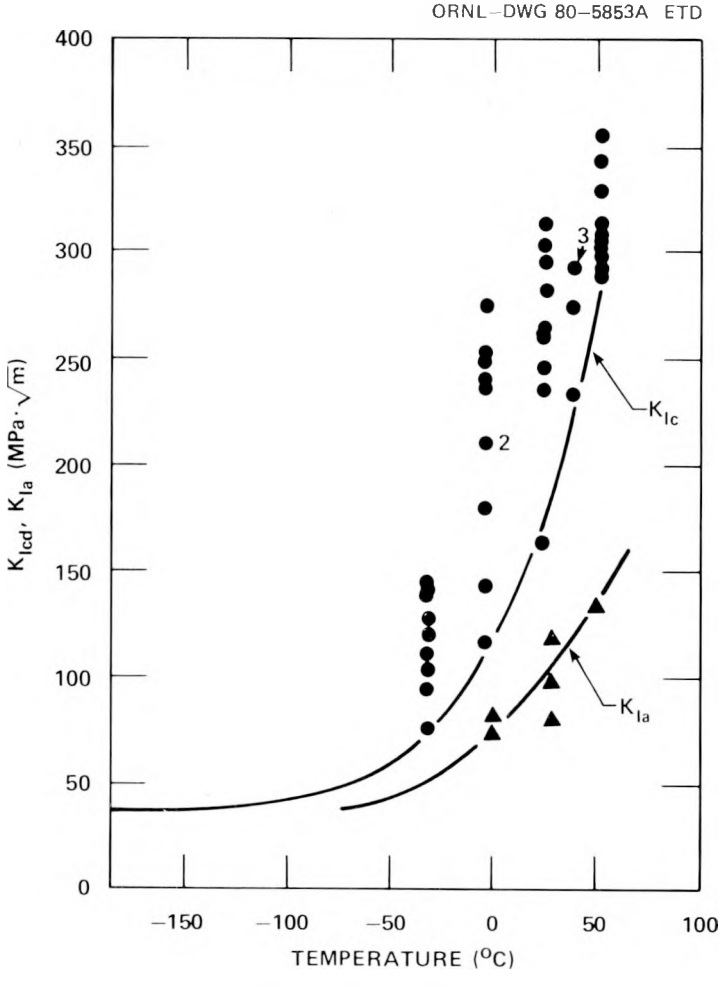

Fig. 4.5. K_{Icd} and K_{Ia} data for TSC-2 prolongation tempered at 677°C.

best estimates of the lower bound for the K_{Ic} data and the mean for the K_{Ia} data and are the curves used in the final pretest analysis of TSE-5A.

The static fracture-toughness data points in Fig. 4.5 were obtained from 1T compact specimens (CSs) using the equivalent-energy technique.* Note that very few of the data points fall close to the lower bound curve. However, the results of TSE-5 (Ref. 5) indicate rather clearly that long flaws will behave in accordance with lower-bound toughness. Relatively few K_{Ia} specimens were used to obtain the K_{Ia} curve in Fig. 4.5 because the scatter in K_{Ia} data was believed to be much less than in K_{Icd}; Battelle Columbus Labs obtained these data using 152.4 × 152.4 × 25.4-mm K_{Ia} compact specimens and our material.

4.5 Surface-Coating Development Studies and Coating of TSC-2 Inner Surface for TSE-5A

By coating the inner surface of the cylindrical test specimens with a thin layer of insulating material, film boiling is suppressed and nucleate boiling promoted during a quench in liquid nitrogen. There is an optimum coating thickness, and the heat transfer coefficient is further enhanced by providing a high-surface density of nucleation sites. Coating development efforts leading up to the application of this technique to TSE-5 are discussed in Ref. 6, and Ref. 3 discusses post-TSE-5 efforts to modify the technique to eliminate blistering that occurred during the latter part of or only after completion of the thermal shock experiments.

As mentioned in Ref. 3, following TSE-5 3M (Ref. 7) personnel recommended that coating material 3M-34 (rather than 3M-NF34, which was used for TSE-5), be used because its chemical composition was much more consistent and it presumably has better adhesive properties under our thermal shock conditions. Preliminary small-scale experiments with 3M-34 resulted in less rapid quench rates than desired, and it appeared, based on these results and an examination of the coating, that there were too few nucleation sites. An attempt to increase the number of sites resulted in excessive webbing.† Webbing had been encountered with 3M-NF34 but to a much lesser extent for presumably the same surface density of nucleation sites. Because the surface coating is applied in many layers, 3M-34 was applied for the first layer to achieve maximum adhesion and then 3M-NF34 for the remaining layers to achieve a high surface density of nucleation sites. This technique was applied to TSC-2 for the pre-TSE-5A full-scale heat-transfer test (TSH-5A-1) discussed in Sect. 4.1. Results of this experiment indicated that the nucleation-site density still was not great enough, and, furthermore, there was some posttest blistering.

---

*Values of static fracture toughness K_{Icd} reported in this chapter are calculated in accordance with the expressions given in American Society for Testing and Materials (ASTM) E 399, with the load P_Q being given by $\sqrt{2kE_{max}}$, where k is the slope of the linear portion of the load-displacement record and E_{max} is the area under the record up to maximum load.

†Threads or strings of coating form on the gun and are cast onto the coated surface creating nonuniformities.

Based on our coating development studies, the surface density of nucleation sites can be increased by decreasing the amount of material sprayed per coat and by increasing the included angle of the spray fan. However, the latter approach is limited by webbing. Thus, for TSE-5A the number of coats was increased to produce a final specified surface density of coating material. The number of coats required could be estimated from previous spray-test data, and thus no additional pre-TSE-5A full-scale heat-transfer tests were conducted.

For TSE-5A, 13 coats were applied to the inner surface of TSC-2 for a total coating surface density of 270 g/m^2, and the final coating appeared to have a high surface density of nucleation sites. Table 4.1 contains information pertinent to the coating application. As a matter of comparison, the coating surface densities for TSE-5 and TSH-5A-1 were 360 and 240 g/m^2. Because all three coatings were thicker than optimum, the quench rate should have increased with decreasing surface density, everything else being equal. The quench rates for TSE-5 and TSH-5A-1 are compared in Fig. 4.1; and, as mentioned in Sect. 4.1, the crossing of the two curves presumably is a result of a relatively low concentration of nucleation sites for the TSH-5A-1 coating.

4.6 TSE-5A

4.6.1 Pretest analysis

Thermal shock experiment TSE-5A is the most recent in a series of six thermal shock experiments designed to reveal the behavior of inner-surface flaws in thick-walled steel cylinders subjected to severe thermal shock loading conditions. The first four experiments (TSE-1, -2, -3, -4)[8] were conducted with A508, class 2 chemistry steel cylinders having a quench-only heat treatment (quenched in water from ~871°C) that provided degraded properties similar to those resulting from extensive radiation damage. The thermal shock was achieved by quenching the inner surface of the cylinder, initially at 288°C, with an alcohol-water mixture at −24°C under forced convection conditions. The dimensions of the test cylinders (533 mm OD × 152 mm wall × 914 mm length) were such that only shallow flaws [fractional crack depth (a/w) <0.2] could be considered.

To include deeper flaws in our studies it was necessary to increase the diameter of the test cylinder so as to increase the flexibility of the wall. The set of test-cylinder dimensions selected (991 mm OD × 152 mm wall × 1220 mm length), coupled with more nearly typical properties for unirradiated material and a thermal shock quench from 93°C in liquid nitrogen, appeared to be suitable for TSE-5 and subsequent experiments. TSE-5 was designed to include a series of initiation-arrest events, arrest in a rising K_I field (K_I increasing with increasing crack depth) and warm prestressing, with a final arrested crack depth in the range of a/w = 0.5–0.7.

A pretest materials-characterization study for TSE-5 was conducted to determine the appropriate tempering temperature for the A508, class 2–chemistry material, and the resultant temperature was 613°C. The results

Table 4.1. Surface-coating data for TSE-5A[a]

Coat No.	Time (d:h:min)	Material	Air press (kPa)	Liquid press (kPa)	Air valve setting (deg)	Liquid valve setting (deg)	Room temperature (°C)	Cylinder temperature (°C)	Quantity sprayed (g)	Surface density (g/m^2)
1	253:11:55	3M-34	410	69	90	360	25	32	430	
2	12:55	3M-NF34	410	48	225	360	26	32	270	
3	13:34	3M-NF34	410	48	225	360	26	32	230	
4	14:00	3M-NF34	410	48	225	360	27	32	230	
5	14:30	3M-NF34	410	48	225	360	27	32	230	
6	15:00	3M-NF34	410	48	225	360	27	32	230	124
7	15:40	3M-NF34	410	48	225	360	27	32	210	
8	16:00	3M-NF34	410	48	225	360	28	32	230	
9	16:30	3M-NF34	410	48	225	360	28	31	230	
10	17:00	3M-NF34	410	48	225	450	28	31	400	
11	17:00	3M-NF34	410	48	225	450	28	31	390	220
12	254:10:11	3M-NF34	410	48	225	450	26	31	480	
13	10:38	3M-NF34	410	48	225	360	24	31	230	270

[a]Spray gun: Binks Model 7R with 36 × 36 SD orifice combination; fan orientation: vertical; rotation rate: 210 rpm; translation rate: 0.014 m/s.

of TSE-5 and an extensive posttest materials-characterization study indicated that this tempering temperature was too low and that the long flaw in TSE-5 behaved in accordance with the lower bound of the final set of K_{Ic} vs temperature data derived from 1T and 2T-CSs. The effective toughness for TSE-5 was too low to permit a demonstration of arrest in a rising K_I field and of warm prestressing, and crack penetration was somewhat deeper than had been expected (a/w = 0.8). TSE-5A is intended to achieve the goals set forth for TSE-5.

The tempering temperature for the TSE-5A test cylinder (TSC-2) was established on the basis of extensive pretest materials-characterization and fracture-mechanics studies. In the materials-characterization studies, ten 1T CSs were tested at each of five test temperatures to establish a "lower-bound" K_{Ic} vs temperature curve for tempering temperatures of 677 and 704°C (the 613°C data were also available for comparison). A tempering temperature of 679°C was finally selected. Data for a tempering temperature of 677°C are shown in Fig. 4.5.

Test conditions for TSE-5A are summarized in Table 4.2; and the nominally expected behavior of the long axial flaw is illustrated graphically in Fig. 4.6, which is a set of critical-crack-depth curves (a_c/w vs time) corresponding to the thermal shock achieved during TSE-5 and the toughness curves shown in Fig. 4.5. Figure 4.6 includes the locus of points

Table 4.2. Test conditions for TSE-5A

Test specimen	TSC-2
Test specimen dimensions, m	
OD	0.991
ID	0.686
Length	1.22
Test specimen material	A508 Class 2 chemistry
Test specimen heat treatment	Tempered at 679°C for 4 h
K_{Ic} and K_{Ia} curves used in design analyses	Lower bound of data from ORNL and BCL TSE-5A materials-characterization studies
Flaw	Long axial sharp crack, a = 11 mm
Temperatures, °C	
Wall (initial)	96
Sink	−196
Coolant	LN_2
Flow conditions	Natural convection
Coating on quenched surface	Rubber cement (3M-NF34)
Coating surface density, g/m^2	270

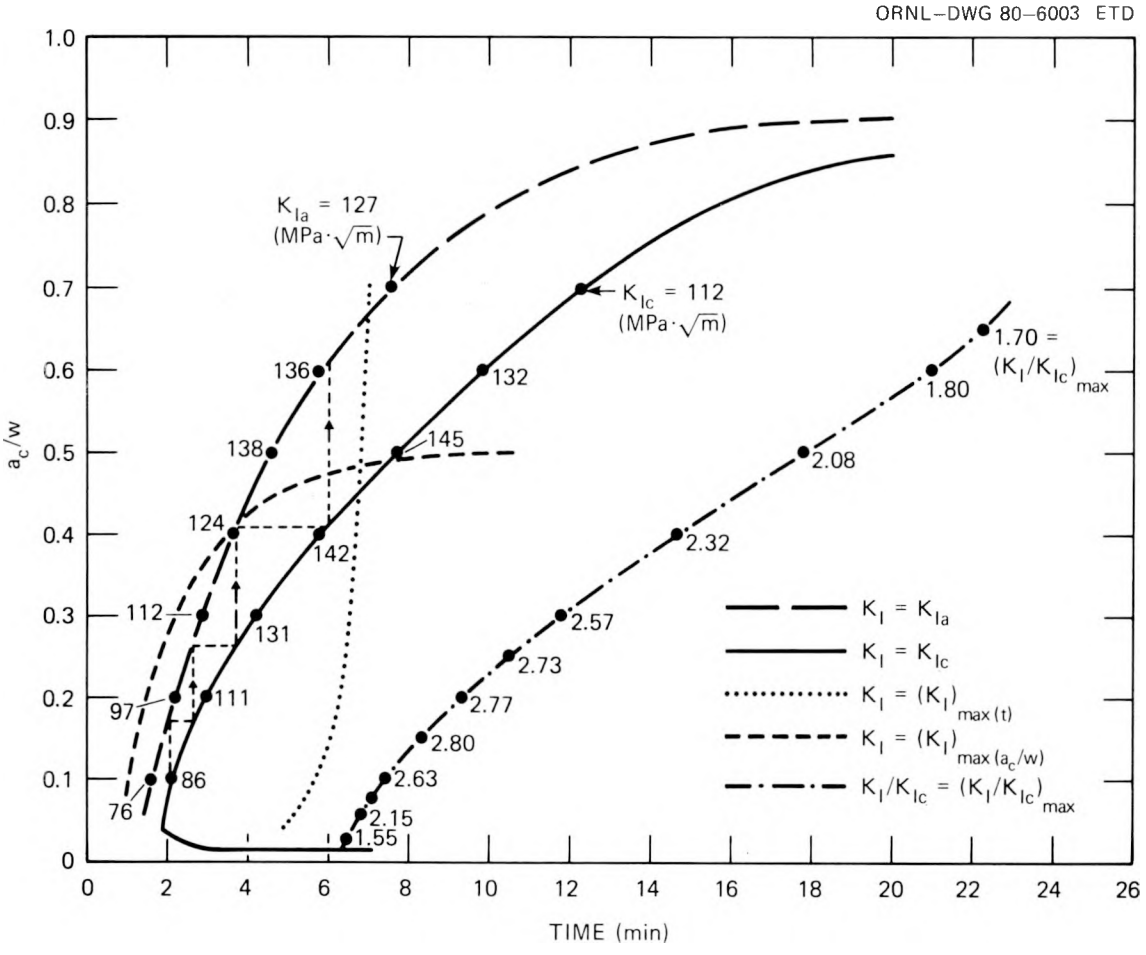

Fig. 4.6. Pretest critical-crack-depth curves for TSE-5A assuming TSE-5 thermal transient and TSE-5A lower-bound K_{Ic} and K_{Ia}.

for $K_I = K_{Ic}$ (initiation curve), $K_I = K_{Ia}$ (static arrest curve), $K_I = (K_I)_{max(t)}$* (warm prestress curve), $K_I = (K_I)_{max(a/w)}$,† and $(K_I/K_{Ic}) = (K_I/K_{Ic})_{max}$,‡ with a few values of K_{Ic}, K_{Ia}, and $(K_I/K_{Ic})_{max}$ included on the appropriate curves. The dashed line represents the expected path of events, starting with initiation of the initial flaw ($a/w \cong 0.08$) at a time of 2 min and ending, after four successive initiation events, with a

---

* $\frac{d(K_I)}{dt} = 0.$

† $\frac{d(K_I)}{d(a/w)} = 0.$

‡ $\frac{d(K_I/K_{Ic})}{dt} = 0.$

final arrest event at a/w = 0.61 and t = 6 min. If warm prestressing were not effective, additional initiation events would take place and the final crack depth would be greater (a/w ≈ 0.9).

The $K_I = (K_I)_{max(a/w)}$ curve in Fig. 4.6 indicates whether arrest must take place in a rising K_I field. For crack depths below this curve, K_I is increasing with crack depth. Thus, the first two predicted arrest events must take place in a rising K_I field.

Design of the thermal shock experiments must account for the uncertainties in K_{Ic}, K_{Ia}, and the liquid-nitrogen film heat-transfer coefficient. Reasonable variations in these parameters were included in a sensitivity analysis to help define limits of acceptability for a successful TSE-5A experiment. Prior to the completion of the pretest TSE-5A materials-characterization and heat-transfer studies, the TSE-5-design K_{Ic} and K_{Ia} curves (ASME Section XI, Appendix A, with RT_{NDT} = −34°C) were used with variations corresponding to RT_{NDT} = −18°C and −1°C. With regard to heat transfer, the TSE-5 design transient, the actual thermal transient and also the most severe thermal transient we considered to be achievable were used (the actual TSE-5 thermal shock was more severe than the design thermal shock). Following completion of the materials-characterization studies and the most recent full-scale heat-transfer experiment, a new set of toughness curves with shifts of ±17 K and a new set of quench data were included. The results of the corresponding fracture-mechanics analyses are summarized in Table 4.3 to indicate the acceptability of a given set of conditions.

To judge the acceptability of a particular set of test conditions, permissible extreme values of $(a/w)_{IWPS}$, $(a/w)_{max}$, $(K_I/K_{Ic})_{max}$, $[(K_I/K_{Ic})_{max}](a/w)_i$, $(NA)_R$, and K_I corresponding to initiation events were established. These factors are identified in Fig. 4.7 and are defined as follows: The factor $(a/w)_{IWPS}$ is the fractional crack depth corresponding to incipient warm prestressing (IWPS), and the minimum acceptable value is ~0.30. The factor $(a/w)_{max}$ is the maximum crack depth at which arrest could take place, assuming warm prestressing (WPS) to be effective, and its maximum acceptable value is 0.75; its minimum value is $(a/w)_{IWPS}$. The factor $(K_I/K_{Ic})_{max}$ is the maximum K ratio (with respect to time) corresponding to $(a/w)_{IWPS}$ and to $(a/w)_{max}$; its minimum acceptable value is 1.7. These first three parameters are determining factors in an adequate demonstration of WPS. The fourth parameter, $[K_I/K_{Ic})_{max}](a/w)_i$, is the maximum K ratio (with respect to time) corresponding to the initial crack depth and is simply an indication of the potential for initiation of the flaw; its acceptable minimum value is 1.5. The next factor, $(NA)_R$, is the number of predicted arrest events that take place in a rising K_I field; the minimum acceptable value is 1. Finally, K_I corresponding to initiation events has been assigned a maximum acceptable value of 165 MPa$\cdot\sqrt{m}$ to minimize nonlinear effects. The values of K_I listed in Table 4.3 are the maximum values along the initiation curve (see typical distribution in Fig. 4.6).

If we assume that the TSE-5A lower-bound toughness curve is accurate within ±17 K, an examination of Table 4.3 shows that a thermal shock at least as severe as that achieved during TSE-5 is required for TSE-5A. The rubber-cement coating for TSE-5A was designed to give a more severe shock,

Table 4.3. Summary of results from TSE-5A sensitivity analysis

K_{Ic} (source)	RT_{NDT} (°C)	$(a/w)_{IWPS}$[a]	$(a/w)_{max}$[b]	$(K_I/K_{Ic})_{max}$[c]	$[(K_I/K_{Ic})_{max}]_{(a/w)_i}$[d]	$(NA)_R$[e]	K_I (MPa·√m)[f]
			TSE-5 design thermal shock				
ASME XI[g]	−34.4	0.49	0.49–0.70	2.1–1.7	2.3	2	126
ASME XI	−17.8	0.59	0.59–0.79	2.2–1.5	2.4	2	125
ASME XI	−1.1	0.70	0.70–0.86	2.0–1.3	2.4	1	121
			TSE-5 actual thermal shock				
ASME XI	−34.4	0.44	0.44–0.62	2.6–2.1	2.8	2	144
ASME XI	−17.8	0.53	0.53–0.74	2.6–1.9	2.8	1	145
ASME XI	−1.1	0.62	0.62–0.84	2.6–1.6	2.9	0	143
TSE-5A[h]	−34.4	0.38	0.38–0.56	2.1–1.7	2.3	3	145
TSE-5A	−17.8	0.45	0.45–0.66	2.2–1.7	2.4	2	145
TSE-5A	−1.1	0.55	0.55–0.75	2.2–1.6	2.5	2	145
			TSH-5A-1 thermal shock				
ASME XI	−34.4	0.37	0.37–0.54	2.1–1.8	2.1	3	124
ASME XI	−17.8	0.45	0.45–0.68	2.2–1.6	2.1	1	125
ASME XI	−1.1	0.56	0.56–0.78	2.2–1.5	2.2	0	125
TSE-5A	−34.4	0.27	0.27–0.41	1.7–1.5	1.7	3	120
TSE-5A	−17.8	0.36	0.36–0.54	1.8–1.5	1.8	2	124
TSE-5A	−1.1	0.47	0.47–0.67	1.9–1.5	2.0	1	126
			Maximum attainable thermal shock				
ASME XI	−34.4	0.39	0.39–0.52	2.9–2.4	3.5	1	180
ASME XI	−17.8	0.43	0.43–0.59	3.0–2.4	3.6	0	180
ASME XI	−1.1	0.50	0.50–0.69	3.1–2.5	3.6	0	182

[a] Fractional crack depth corresponding to IWPS.

[b] Range of maximum crack penetration (fractional), assuming WPS to be effective.

[c] Range of $(K_I/K_{Ic})_{max}$ corresponding to range in final crack depth defined in footnote *b* above.

[d] $(K_I/K_{Ic})_{max}$ corresponding to initial flaw ($a/w \approx 0.083$).

[e] Number of arrest events with positive value of $d(K_I)/d(a/w)$.

[f] Maximum values of K_I corresponding to predicted initiation events (see Fig. 4.6).

[g] Toughness curve defined in ASME Section XI, Appendix A.

[h] Toughness curves defined in Fig. 4.5. (For convenience, curves shown in Fig. 4.5 were assigned a value of RT_{NDT} equal to −17.8°C. Actual RT_{NDT} not specified.)

and we expected at least as severe a shock as that in TSE-5. The severity certainly would not be greater than that achieved with the maximum attainable thermal shock, which would be satisfactory except for demonstrating arrest in a rising K_I field.

Note that TSH-5A-1 (a heat-transfer experiment) was conducted to show that we could in fact achieve the desired thermal shock for TSE-5A. The result of the experiment, compared to TSE-5, was more rapid cooling during

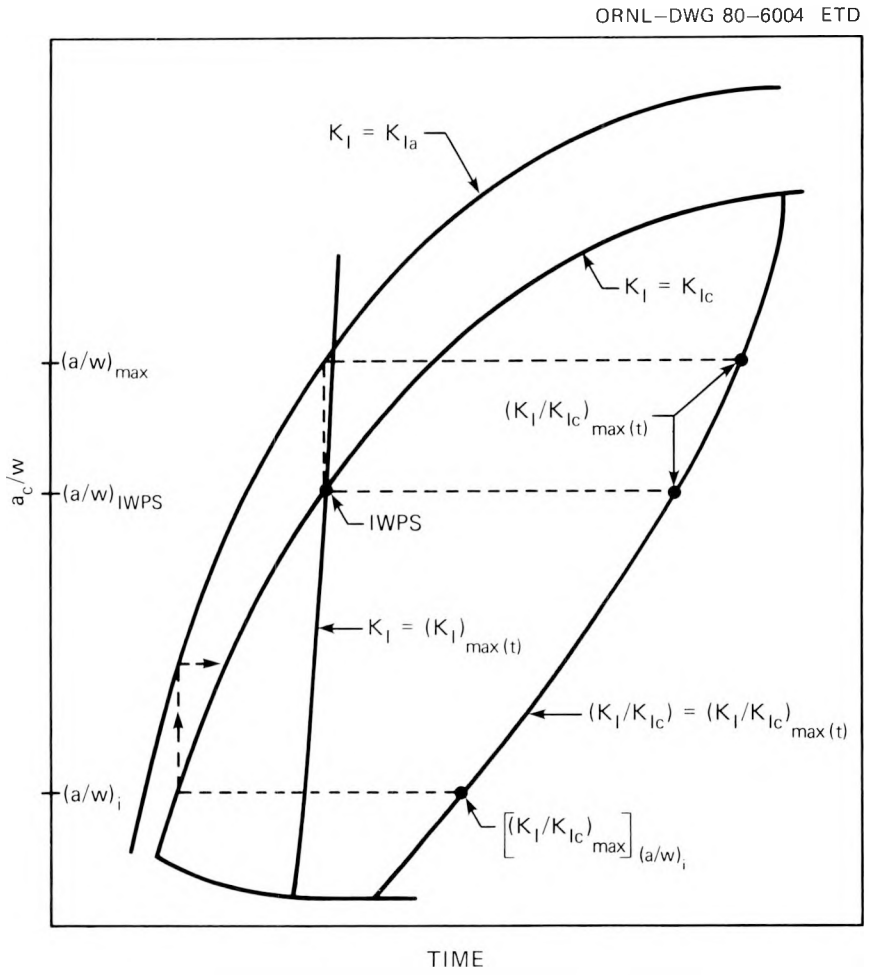

Fig. 4.7. Critical-crack-depth curves showing various parameters used for evaluating acceptance of test conditions.

the first 2.5 min but less rapid cooling thereafter. Since the coating was thinner than that used for TSE-5, the cooling rate should have been greater throughout the transient. It was concluded that there were fewer nucleation sites for TSH-5A-1 than for TSE-5. As a result, changes were made in the coating application technique, and the TSE-5A coating was believed to have an adequate number of nucleation sites.

In summary, the desired crack behavior for TSE-5A appeared to be achievable if the TSE-5A thermal shock was at least as severe as that achieved during TSE-5 and if the effective toughness curve (K_{Ic} vs temperature) for the test-cylinder material was within ± 17 K of the lower-bound curve defined in Fig. 4.5. Based on the results of TSE-5, full-scale heat-transfer experiments conducted in the liquid-nitrogen test facility, and extensive TSE-5A materials-characterization studies, these conditions were believed to be achievable.

4.6.2 TSE-5A results

Thermal shock experiment TSE-5A was conducted on Sept. 24, 1980. As predicted, there were four initiation-arrest events, and the maximum fractional final flaw depth, based on ultrasonic (UT) measurements, appeared to be 0.53, close to the expected value. Times for the events were less than those indicated in Fig. 4.6, and this too was expected because an attempt was made to achieve a thermal shock more severe than that associated with Fig. 4.6 (TSE-5 quench rate). A comparison of the inner-surface quench rates for TSE-5A and TSE-5 is shown in Fig. 4.8, and the number and time of initiation-arrest events, as detected with seven crack-opening displacement (COD) gages that straddled the flaw, are shown in Fig. 4.9. Based on a preliminary examination of available data, a fifth initiation event apparently was prevented by warm prestressing, and the maximum value of (K_I/K_{Ic}) for the final flaw depth was ~2.0, which is quite satisfactory for a convincing demonstration of warm prestressing. A detailed posttest analysis for TSE-5A is under way.

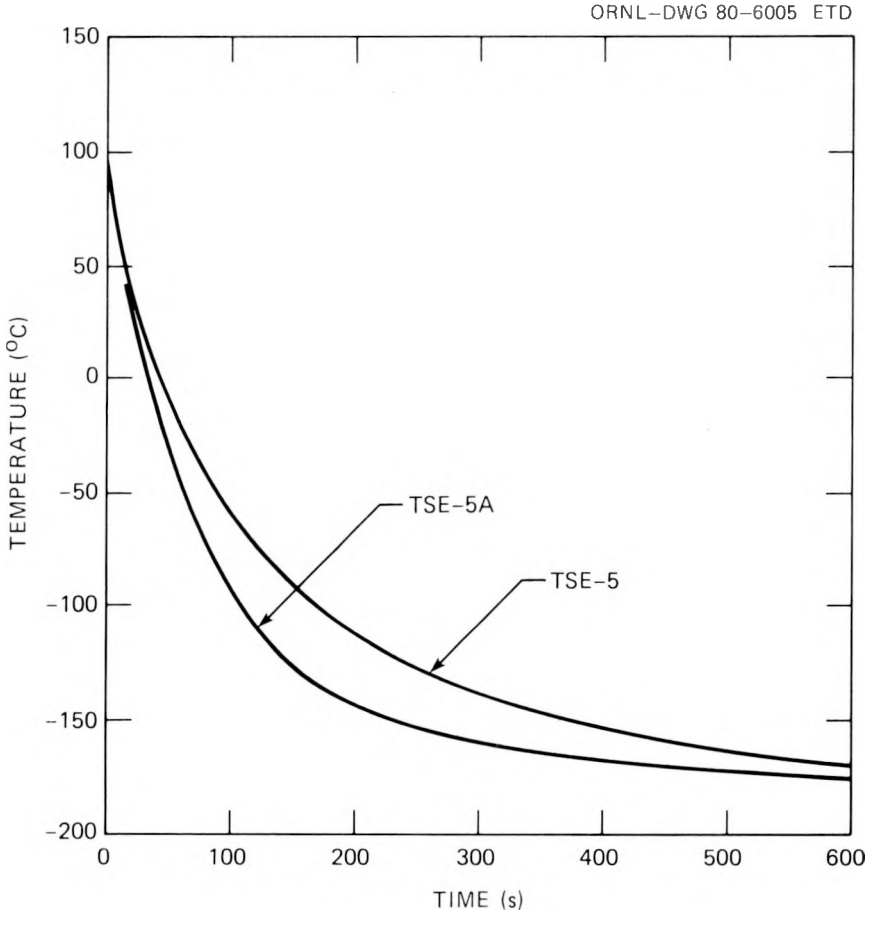

Fig. 4.8. Comparison of inner-surface (a/w = 0.0083) quench rate for TSE-5 and TSE-5A.

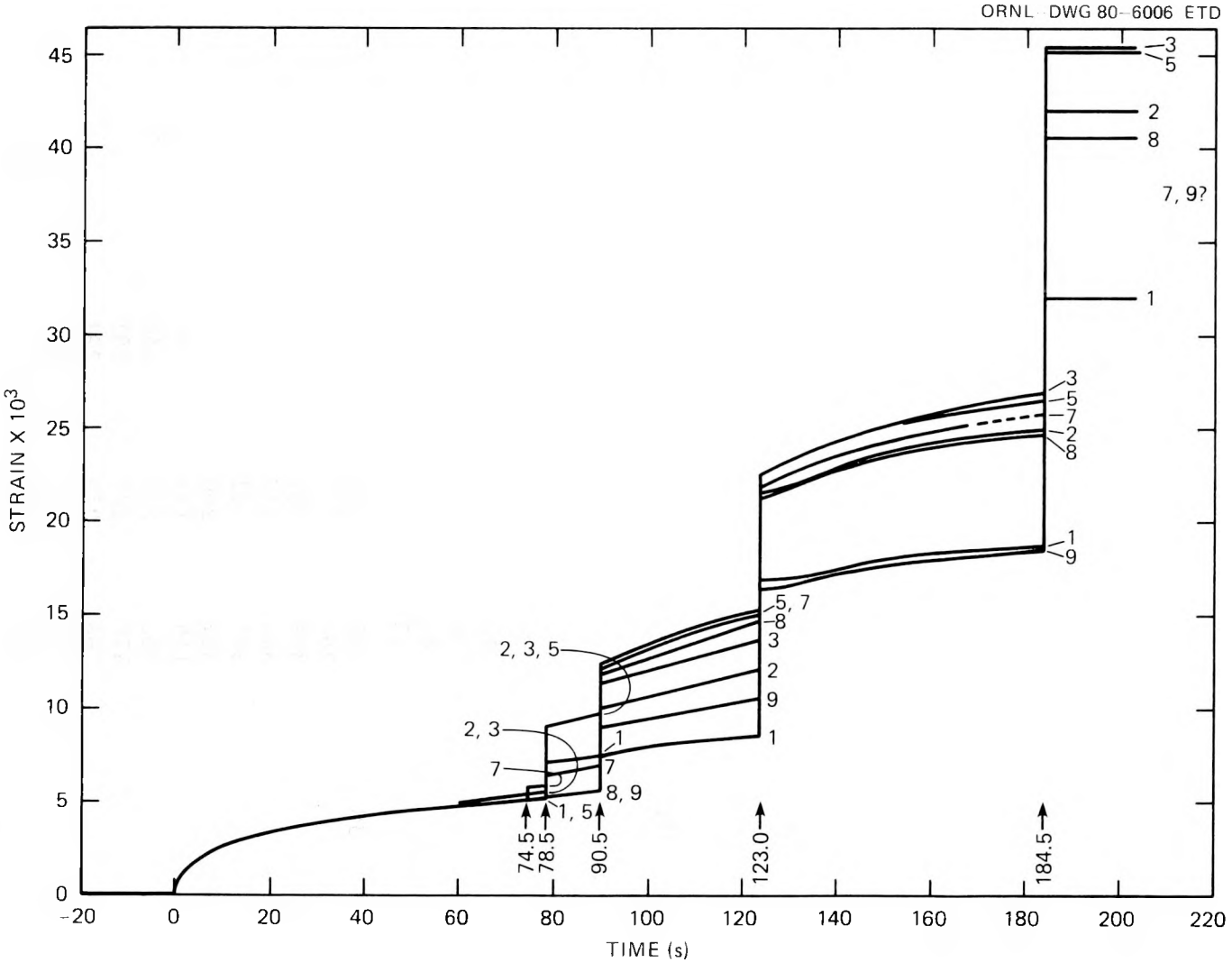

Fig. 4.9. COD data for TSE-5A.

4.7 Thermal Shock Materials Characterization

W. J. Stelzman D. A. Canonico

We have completed testing of CT-oriented 1T CSs from a segment of thermal shock prolongation, TSP-2, after the prolongation had received the same temper as test vessel TSC-2 (4 h at 679°C). Twenty-two specimens were tested: 10 at −32°C and 12 at 38°C. The results are summarized in Table 4.4. Six of the specimens tested at 38°C and one of the specimens tested at −32°C were unloaded prior to fracture and analyzed in accordance with the proposed ASTM standard method for determination of elastic-

Table 4.4. Static fracture toughness from 1T CSs[a] of quenched prolongation TSP-2 after tempering at 680°C for 4 h and air cooling

Test temperature (°C)	J (kJ/m²)	K_J (MPa $\sqrt{m}$)	K_{Icd} (MPa $\sqrt{m}$)	Average crack extension (μm)
−32	92[b]	138[b]	145[b]	58
	34[b]	84[b]	87[b]	0
	40	91	94	41
	55	106	111	56
	70	121	126	58
	65	116	120	48
	48	99	102	36
	83	131	137	69
	88	135	141	76
	25	72	75	0
38	246	226	238	241
	367	276	294	653
	308	252	266	320
	346	267	281	472
	383	282	299	551
	327	260	273	559
	115	154	160	69
	262	233	244	277
	371	277	292	14,500
	366	275	292	8,780
	233	220	231	432
	382	281	296	3,640

[a] CT-oriented specimens.

[b] Specimens unloaded prior to fracture.

plastic toughness parameter, J_{Ic}. The remainder of the specimens were tested to failure. Results of all the tests are included in Table 4.4.

After testing, the crack extension prior to onset of fast fracture was measured for each specimen. This information is also provided in Table 4.4. The J-value versus Δa (crack extension) for the specimens tested are shown in Figs. 4.10 and 4.11. Results from specimens tested at −32°C are shown in Fig. 4.10. Nearly all of the measured crack extensions are on or near the calculated [$J = 2\sigma_y\Delta_a$, where $\sigma_y = (ys + uts)/2$] theoretical blunting line. The values of J and K_J (K-value calculated from J) ranged from 25 to 92 kJ/m^2 for J and 72 to 145 MPa $\sqrt{m}$ for K_J. K_J was calculated from the expression $K_J^2 = EJ$, where E was assumed to be 210 GPa.

Results from specimens tested at 38°C are shown in Fig. 4.11. The six 1T CSs in which the tests were interrupted exhibited crack extensions near the 0.15-mm offset line. Three of the specimens tested to failure exhibited crack extensions too close to the 0.15-mm offset line to permit the construction of a meaningful R-curve. The last three specimens tested to failure underwent a great deal of tearing (>3.6 mm). These results are also plotted in Fig. 4.11. The J-value calculations are based on the area

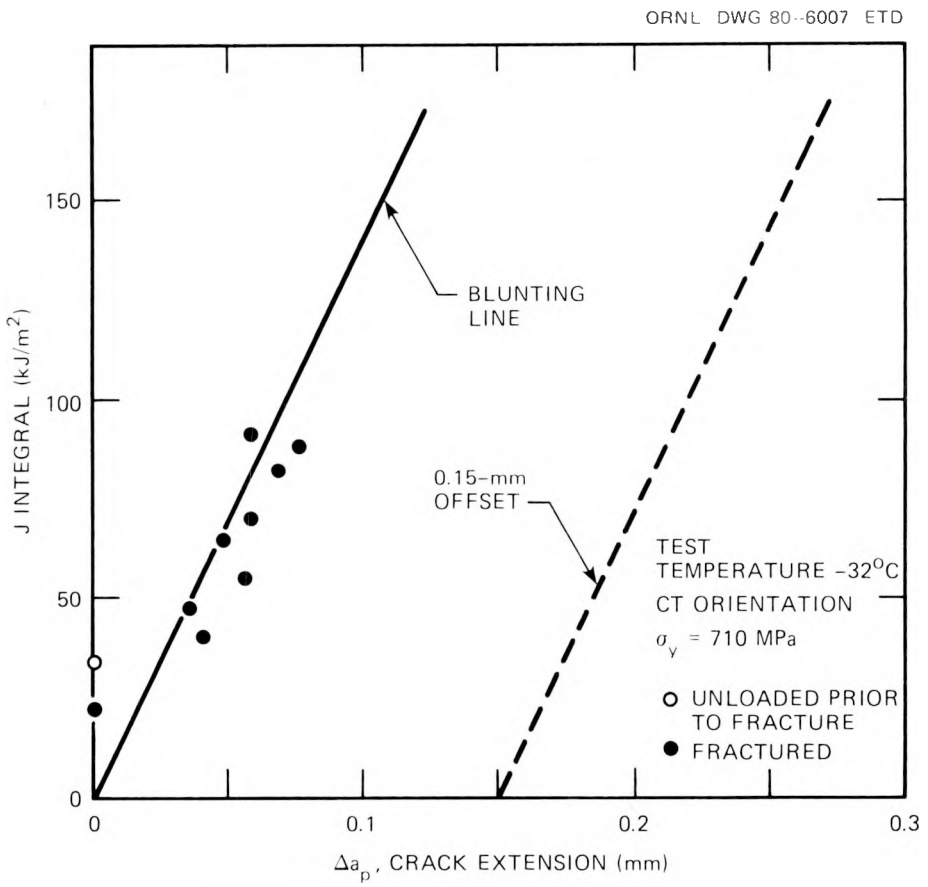

Fig. 4.10. Variation of J integral with stable crack growth for 1T compact specimens from prolongation TSP-2 after tempering at 679°C for 4 h and cooling in air.

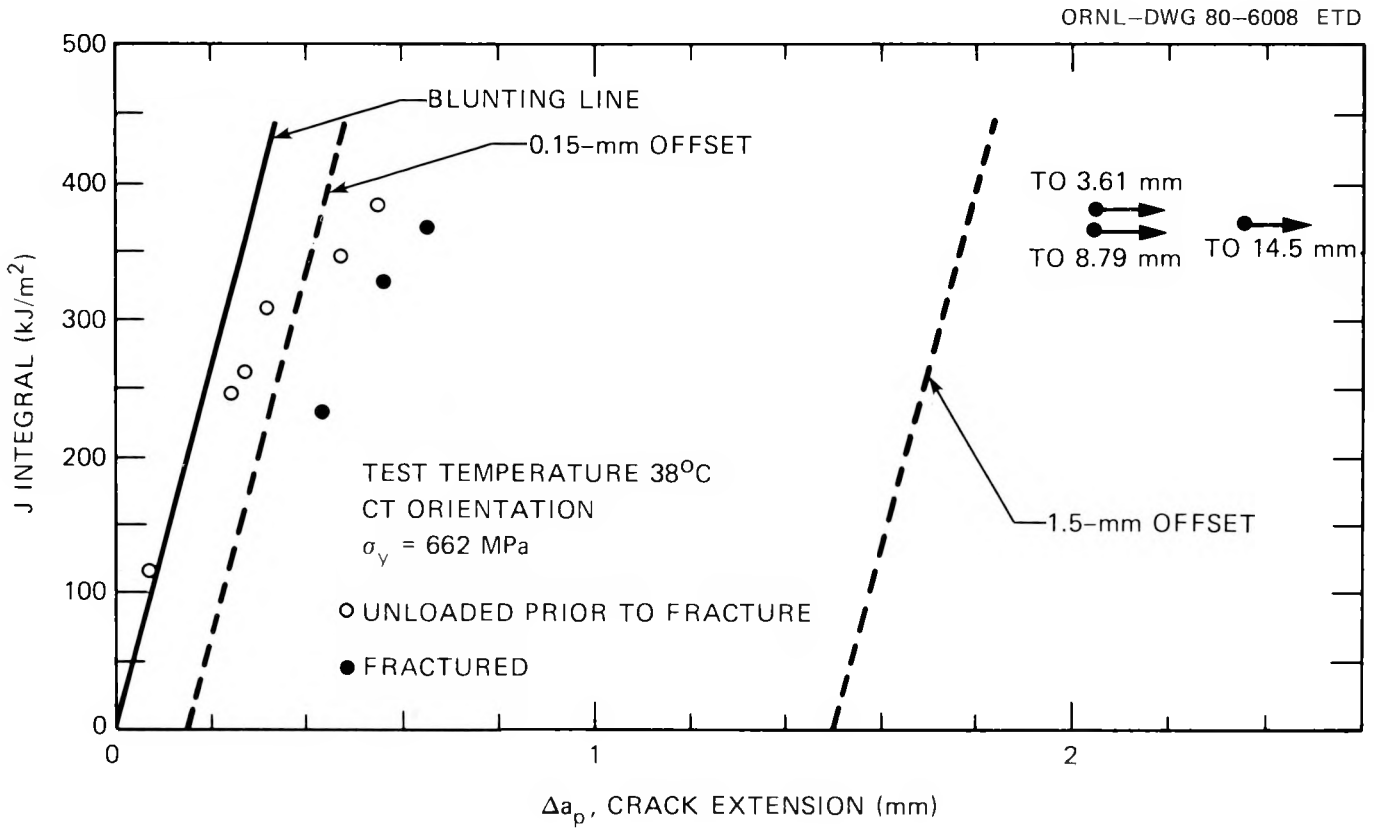

Fig. 4.11. Variation of J integral with stable crack growth for 1T compact specimens from prolongation TSP-2 after tempering at 679°C for 4 h and cooling in air.

under the load-deflection curve to maximum load. These three specimens failed at deflections considerably in excess of those associated with maximum load. The values of J and K_J from the fractured specimens ranged from 233 to 382 KJ/m^2 for J and 220 to 281 MPa $\sqrt{m}$ for K_J.

The results from the 1T CSs tested at −32 and 38°C are included in Fig. 4.12 together with previously reported[9] results from earlier tests.

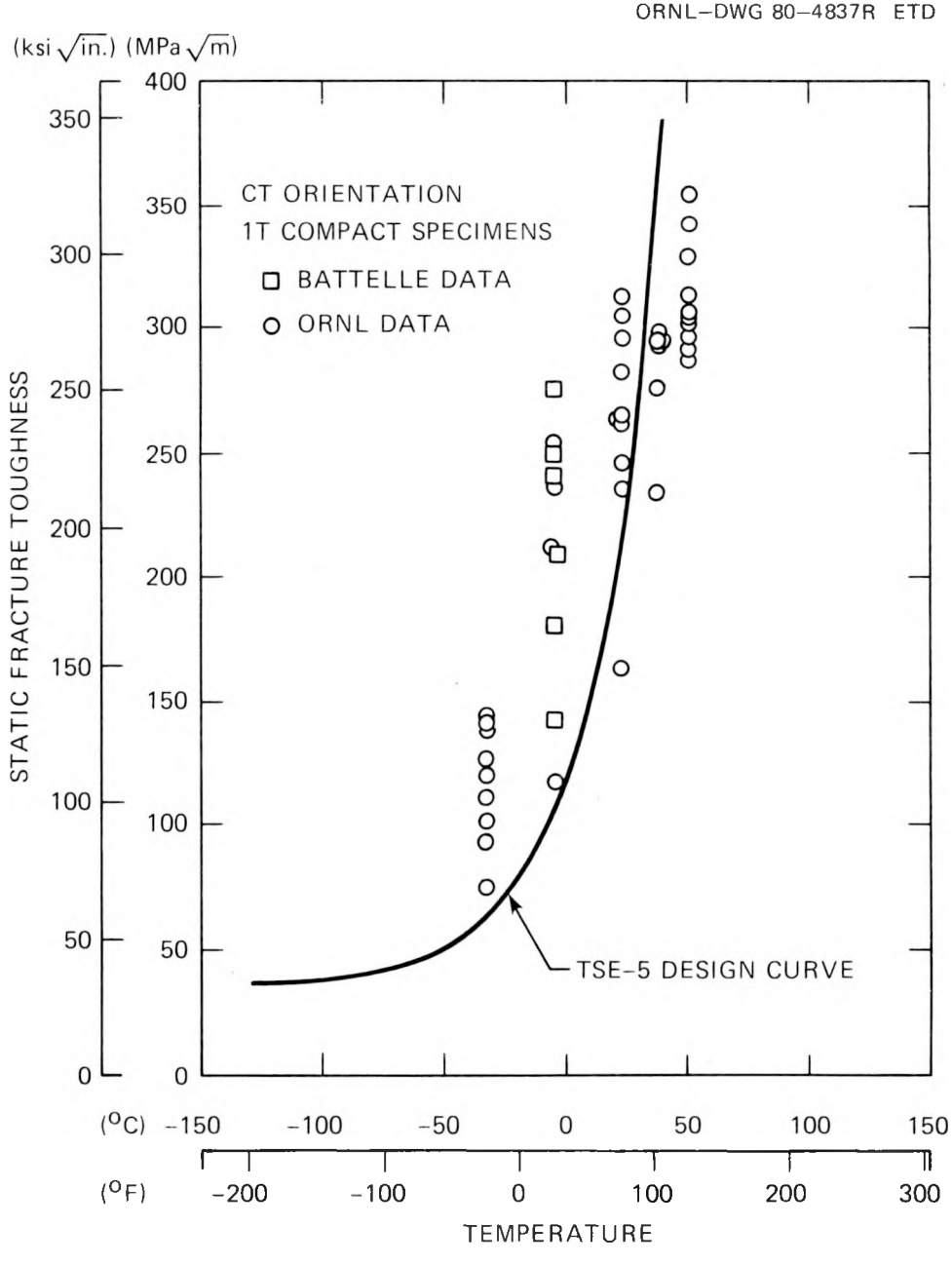

Fig. 4.12. Variation of static fracture toughness from 1T compact specimens from prolongation TSP-2 after tempering at 678°C for 4 h and cooling in air.

References

1. R. D. Cheverton, "Thermal Shock Investigations," *Heavy-Section Steel Technology Program Quart. Prog. Rep. April–June 1979*, NUREG/CR-0980 (ORNL/NUREG/TM-347), pp. 63–67.

2. R. D. Cheverton, "Thermal Shock Investigations," *Heavy-Section Steel Technology Program Quart. Prog. Rep. July–September 1979*, NUREG/CR-1197 (ORNL/NUREG/TM-370), pp. 52–74.

3. R. D. Cheverton, "Thermal Shock Investigations," *Heavy-Section Steel Technology Program Quart. Prog. Rep. April–June 1980*, NUREG/CR-1627 (ORNL/NUREG/TM-401), pp. 28–56.

4. P. P. Holz, *Flaw Preparations for HSST Program Vessel Fracture-Mechanics Testing: Mechanical-Cyclic Pumping and Electron-Beam Weld-Hydrogen-Charge Cracking Schemes*, NUREG/CR-1274 (ORNL/NUREG/TM-369) (May 1980).

5. R. D. Cheverton, "Thermal Shock Investigations," *Heavy-Section Steel Technology Program Quart. Prog. Rep. January–March 1980*, NUREG/CR-1477 (ORNL/NUREG/TM-393), pp. 19–21.

6. R. D. Cheverton, "Thermal Shock Investigations," *Heavy-Section Steel Technology Program Quart. Prog. Rep. April–June 1977*, ORNL/NUREG/TM-147, pp. 69–77; and "Thermal Shock Investigations," *Heavy-Section Steel Technology Program Quart. Prog. Rep. October–December 1977*, ORNL/NUREG/TM-194, pp. 63–73.

7. Don Kennedy, Minnesota-Mining, personal communication to R. D. Cheverton, Apr. 1, 1980.

8. R. D. Cheverton and S. E. Bolt, *Pressure Vessel Fracture Studies Pertaining to a PWR LOCA-ECC Thermal Shock: Experiments TSE-3 and TSE-4 and Update of TSE-1 and TSE-2 Analysis*, ORNL/NUREG-22 (December 1977).

9. W. J. Stelzman and D. A. Canonico, "Thermal Shock Material Characterization," *Heavy-Section Steel Technology Program Quart. Prog. Rep. January–March 1980*, ORNL/NUREG/TM-393, pp. 31–35.

5. PRESSURE VESSEL INVESTIGATIONS

5.1 Intermediate Test Vessel V-8A

R. H. Bryan P. P. Holz

Babcock and Wilcox Company, Alliance Research Center, Alliance, Ohio, under subcontract is nearing the completion of welding trials of the first task in the preparation of intermediate test vessel V-8A for an experiment on fracture of low-upper-shelf welds.[1] Work has just started at their Barberton manufacturing facility on a 150-mm-thick trial weld which is intended to be a demonstration of the welding procedure to be used on intermediate test vessel V-8A. This procedure, selected from nine preliminary automated submerged-arc weld trials, produced the best combination of results in terms of upper-shelf Charpy impact energy level, transition temperature, and tensile properties. The variables for the preliminary trials were flux composition and heat-treatment temperature. Combinations of three compositions and three temperatures provided the nine preliminary trial conditions.

The selected preliminary submerged-arc weld (V8-22) was made with a copper-clad NiMnMo wire of type SFA 5.23EF2 and a 75% Linde 60, 25% Linde 80 flux mixture followed by a 50-h heat treatment at 566 to 593°C. Upper-shelf energies ranged from 50 to 63J (target range 47 to 75J) and tensile yield stresses from 452 to 468 MPa (target range 450 to 620 MPa). These levels are acceptable. However, a slight percentage of cleavage persisted for test temperatures up to 90°C, which may force us to test vessel V-8A somewhat above 100°C. Because such a high-temperature test would be a significant inconvenience, Babcock and Wilcox has explored changes in the procedure that should shift the transition temperature downward to try to attain full upper-shelf behavior at a temperature of 90°C or lower.

They have recommended and we have agreed to two measures. First, the V8-22 procedure being used on the trial weld will have a lower heat input than that used in the preliminary trial. A laboratory trial was made to confirm weldability with the lowered heat input. This change, according to estimates, will diminish the transition temperature by ~15 K. Second, an additional preliminary weld has been made with a slightly different wire. The change in wire composition is estimated to shift the transition temperature downward ~20 K.

5.2 Pressurized Thermal Shock Studies

W. R. Corwin

5.2.1. Introduction

Scoping studies on the behavior of a nozzle-corner flaw in an ITV under internal pressure and thermal shock were concluded. This concept

has been seen as an experimentally viable method to investigate the fracture behavior of an engineering scale structure under combined loading as well as providing an experimental facility for use in a proposed Electric Power Research Institute (EPRI) thermal fatigue test program. Such testing would help establish the capability to predict the structural response of a flawed nozzle or pressure vessel during a transient in which combined pressure and thermal loads were imposed on the structure, such as in a main steam line break in a pressurized-water reactor, a small break loss-of-coolant accident, or an over cooling transient.

Results of the scoping studies, described in detail below, indicated that conditions leading to fracture could be reached in an ITV containing a flawed nozzle corner under reasonable experimental conditions. However, there would be sufficient experimental and analytic uncertainties to make a definitive assessment of the ability of the currently available techniques to quantitatively predict the fracture behavior under other arbitrary conditions of loading, material properties, and geometry very difficult. For this reason, as well as the substantial capital expense of such a facility, using a geometry for which the analytical and experimental requirements are much simpler is being investigated. We are now looking at a cylindrical ITV under internal pressure in which both the flaw and thermal shock would be on the outside of the vessel. To this end, we have initiated conceptual design studies of the required test facility as well as scoping analyses of the response of a hypothetical reactor vessel to various pressurized thermal transients to identify relevant time-temperature-loading histories. First indications are that by using such a test medium the experimental conditions covering the range of interest could be produced in a significantly less complex test facility than for the internal pressure–thermal loading of an ITV nozzle-corner flaw, and at the same time this test medium could provide a system which is more analytically tractable.

5.2.2. Results of analytical scoping studies

Calculations were performed under Task 2 (Ref. 2) using the ADINAT, ADINA, and BIGIF computer codes to determine the local stress intensity factor K_I, caused by combined pressure thermal loading of a flaw in the blend radius of a nozzle in an ITV. The load imposed was that of internal design pressure of the ITV combined with a moderately severe thermal shock to the inside of the vessel in the vicinity of the blend radius (Fig. 5.1). Quarter-circular flaws with depths of 14, 29, and 53% of the local wall thickness were considered.

The resultant K_I values for the geometry, loading, and crack depths considered were shown to be greater along the interior portion of the crack front for the shallowest flaw, whereas for the two deeper flaws the reverse was true (Fig. 5.2). Also, as expected, the length of time after initiation of the thermal shock required to reach a maximum K_I along the crack front generally increases with increasing crack depth (Figs. 5.2 and 5.3). The maximum values of K_I calculated under the conditions investigated approached 225 MPa $\sqrt{m}$.

To determine if a crack advance could occur, the K_I distributions calculated in the above manner were compared with the levels of fracture

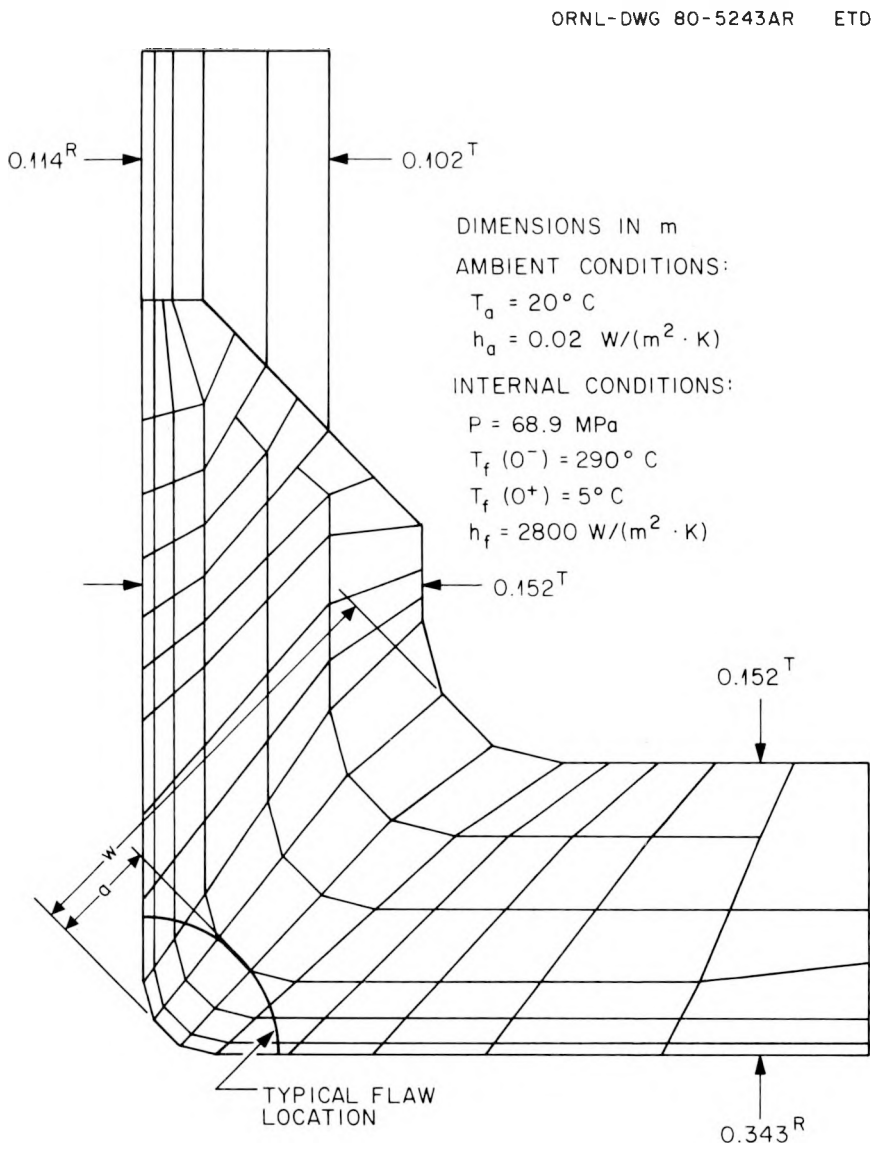

Fig. 5.1. Portion of ITV nozzle area modeled in the pressurized thermal shock loading analysis and showing the boundary conditions utilized, the computer mesh, and a typical quarter-circular flaw.

toughness in the nozzle of a typical reactor pressure vessel steel which would exist at the corresponding times and resultant temperature distributions during the transient (Fig. 5.4). Since the unused ITV V-10 contains a nozzle and would be a prime candidate as a test vessel for such an experiment, the specific material properties used for comparison were those measured[3] on the same forging as that from which the nozzle in V-10 was fabricated[4] (Fig. 5.5).

The results of this linear elastic analysis showed that, over a range of critical combinations of time, crack depth, and position along the crack

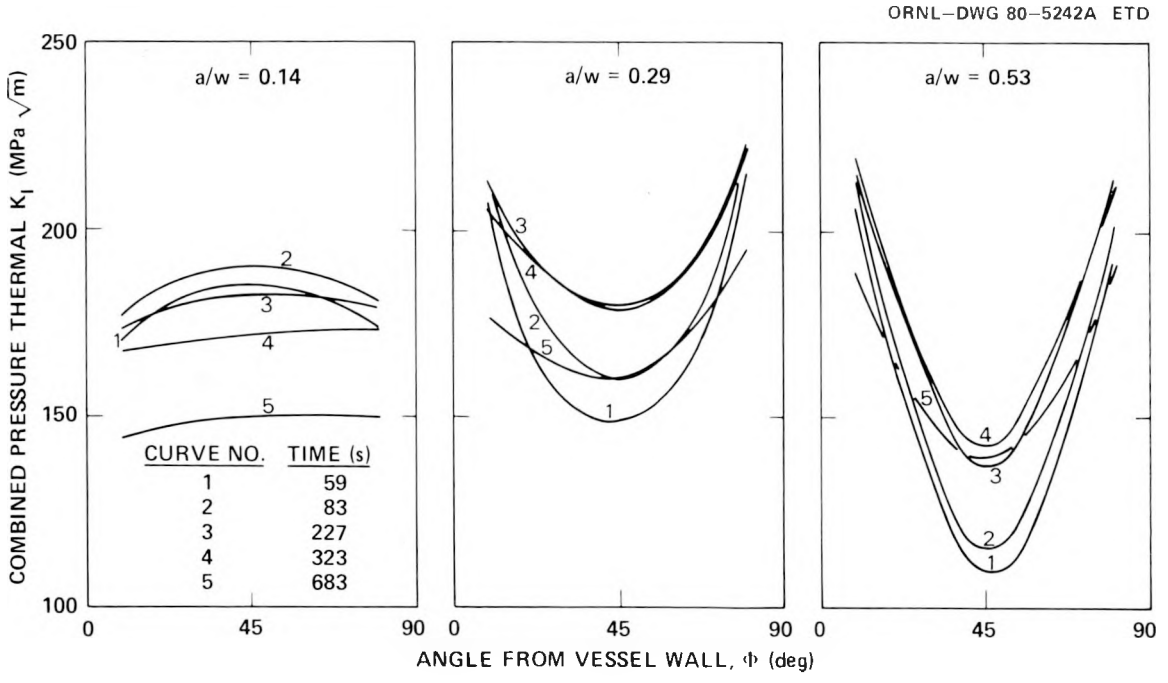

Fig. 5.2. Local values of K_I calculated for three quarter-circular flaws of increasing normalized depth located in an ITV nozzle at various times into a pressurized thermal shock.

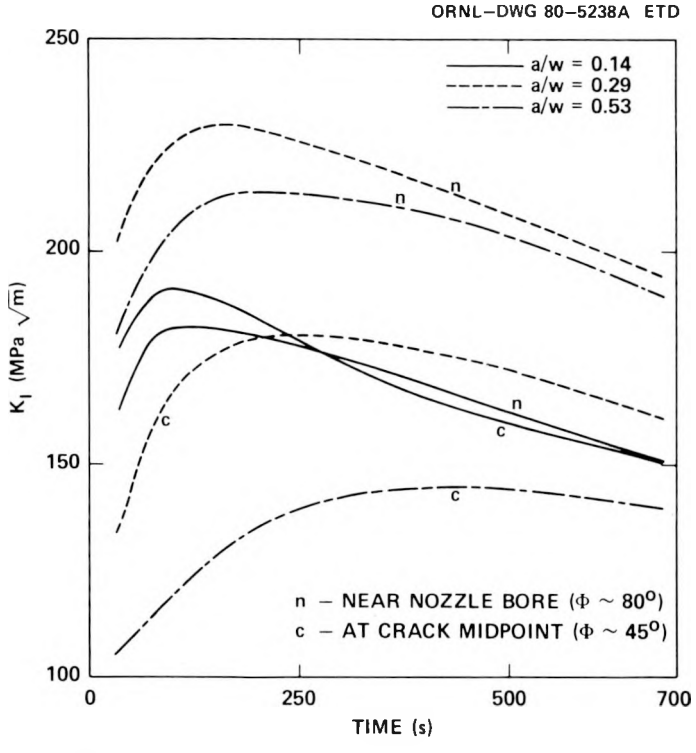

Fig. 5.3. Local values of K_I as a function of time for quarter-circular flaws of three normalized depths located in an ITV nozzle during a pressurized thermal shock.

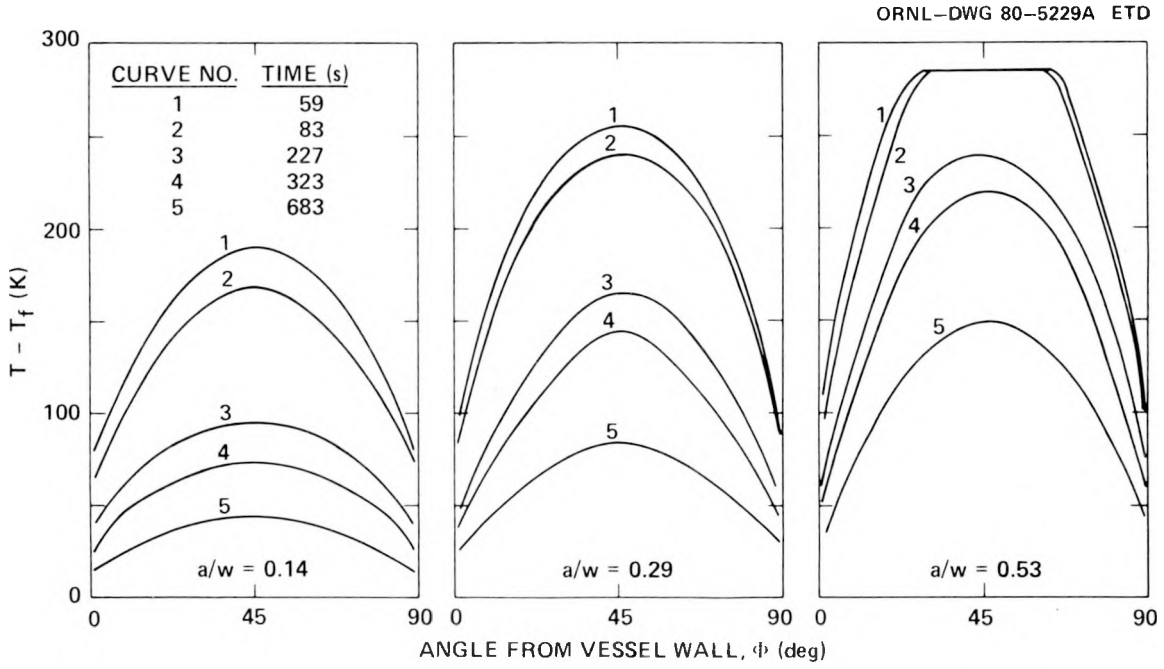

Fig. 5.4. Variation of temperature along the crack fronts of flaws at three normalized depths. T_f = 5°C.

front, the K_I resulting from the combined pressure thermal load will exceed the lower limit of the measured fracture toughness of the nozzle material [Fig. 5.6(a)]. In general, the applied K_I exceeds the material's fracture toughness by the greatest amount near the nozzle bore and vessel wall where material temperature and resultant toughness are lower and by less or not at all along the central portion of the crack front where the material is still warmer and tougher. For the experimental conditions considered, K_I exceeds the fracture toughness of the material when the material is still warm enough that it would very likely be on the upper shelf along virtually the entire crack front. The test could be performed in a regime below the upper shelf by lowering the initial temperature of the vessel. For instance, if the fluid sink temperature were reduced by 30 K (approaching the lower limit of water-based cooling media) and the initial vessel temperature likewise reduced by 30 K (maintaining the temperature differential and thermal stress contribution while lowering the material toughness at a given time into the test) while holding all other experimental conditions constant, then the material near the nozzle bore and vessel wall would be brought into the upper transition range during the times at which its fracture toughness is exceeded [Fig. 5.6(b)]. Moreover, other cases can be readily specified by dropping the initial vessel temperature further and increasing the contribution of the internal pressure as necessary such that crack advance could occur over a wide range of regimes throughout the transition range.

Therefore, based on the preceding linear elastic fracture mechanics analysis, obtaining varying degrees of crack advance is possible, at least

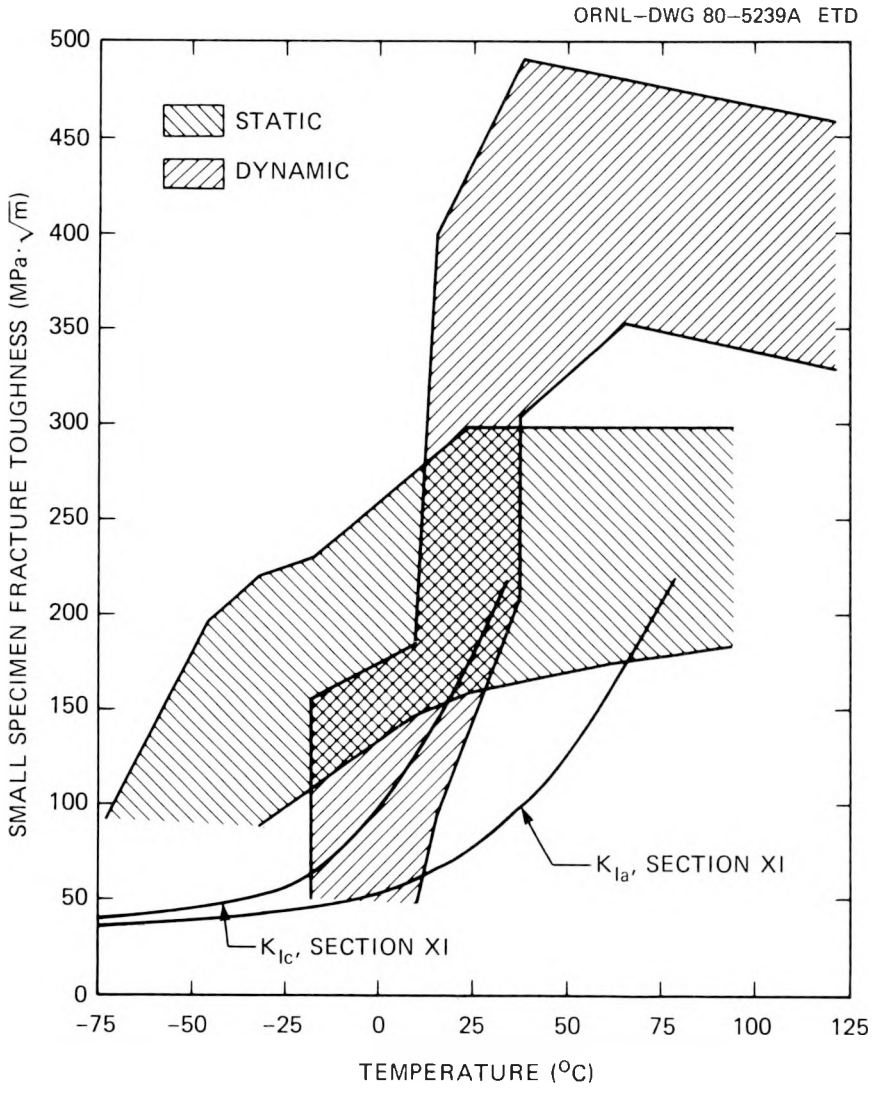

Fig. 5.5. Upper and lower bounds of fracture toughness estimated from static and dynamic small specimen tests conducted on the forging material from which the nozzle in ITV 10 was fabricated. K_{Ia} and K_{Ic} from ASME Code Section XI are shown for comparison.

in the transition region and perhaps on the upper shelf, utilizing a cracked ITV nozzle corner under conditions of internal pressure of the design level or somewhat above and a moderate, simultaneous thermal shock if the lower limit of fracture toughness of the material were controlling. However, before we would feel confident that the ability exists to quantitatively predict the fracture behavior of such a test thereby validating the analytical methods for use in other arbitrary cases, numerous areas of major concern which have been identified in this initial study would have to be satisfactorily addressed. These include (1) the formulation and use of appropriate fracture criteria in the upper-shelf and upper-transition regimes; (2) the elastic-plastic nature of the loading of the structure

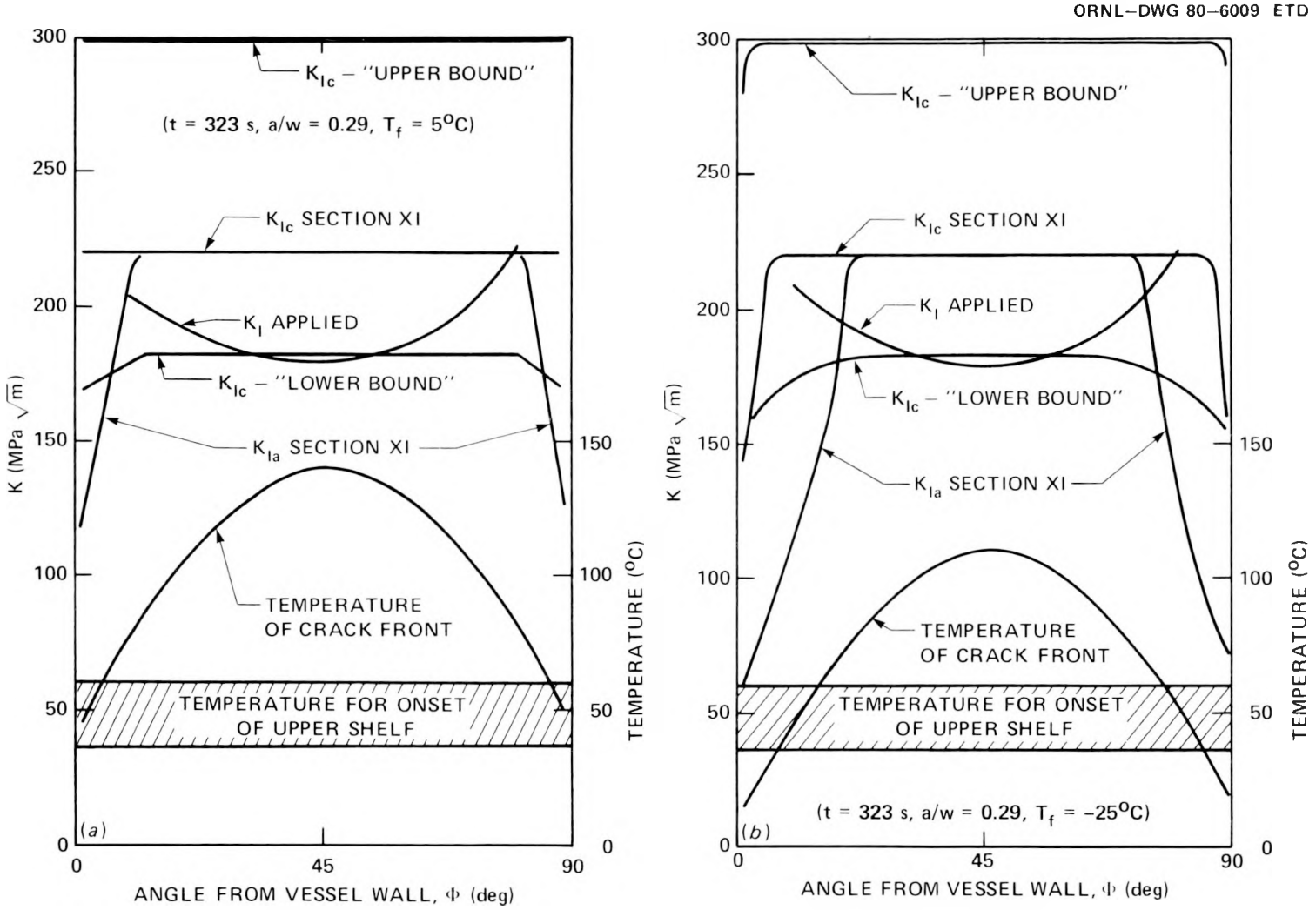

Fig. 5.6. Comparison of the calculated K_I applied by a combined pressure thermal load in a flawed 1TV nozzle corner at 323 s into a pressurized thermal shock experiment with the fracture toughness of the nozzle along the crack front. In (a) where the initial vessel and sink temperatures are 290°C and 5°C respectively, material remains on upper shelf even when its nominal lower bound toughness is exceeded. Dropping initial and sink temperatures by 30 K each in (b) results in bringing the material near the surface into the transition range.

including the variable levels of transverse restraint; (3) the effects of steep gradients in stress, K_I, temperature, and material fracture toughness; and (4) the methods of extrapolation of the results to real cases of interest considering effects of geometry, material embrittlement, and system conditions.

References

1. P. P. Holz, "Intermediate Test Vessel V-8A," *Heavy-Section Steel Technology Program Quart. Prog. Rep. April–June 1980,* NUREG/CR-1627 (ORNL/NUREG/TM-401), pp. 57–58.

2. J. W. Bryson, B. R. Bass, and R. H. Bryan, "Determination of K-Factors for Nozzle-Corner Flaws Under Combined Pressure-Thermal Loading," *Heavy-Section Steel Technology Program Quart. Prog. Rep. April–June 1980,* NUREG/CR-1627 (ORNL/NUREG/TM-401), pp. 3–5.

3. J. G. Merkle, G. C. Robinson, P. P. Holz, and J. E. Smith, *Test of 6-in.-Thick Pressure Vessels. Series 4: Intermediate Test Vessels V-5 and V-9 with Inside Nozzle Corner Cracks,* ORNL/NUREG-7, pp. 25–29 (August 1977).

4. C. E. Childress, *Fabrication and Mechanical Test Data for the Four 6-in.-Thick Intermediate Test Vessels Made from Steel Plate for the Heavy Section Steel Technology Program,* ORNL-TM-5074 (January 1976).

CONVERSION FACTORS[a]

SI unit	English unit	Factor
mm	in.	0.0393701
cm	in.	0.393701
m	ft	3.28084
m/s	ft/s	3.28084
kN	lb_f	224.809
kPa	psi	0.145038
MPa	ksi	0.145038
$MPa \cdot \sqrt{m}$	ksi $\sqrt{in.}$	0.910048
J	ft-lb	0.737562
K	°F or °R	1.8
kJ/m^2	$in.-lb/in.^2$	5.71015
$W \cdot m^{-2} \cdot K^{-1}$	$Btu/hr-ft^2-°F$	0.176110
$T(°F) = 1.8\ T(°C) + 32$		

[a]Multiply SI quantity by given factor to obtain English quantity.

NUREG/CR-1806
ORNL/NUREG/TM-419
Dist. Category RF

Internal Distribution

1. R. G. Berggren
2. S. E. Bolt
3-7. R. H. Bryan
8. J. W. Bryson
9. D. A. Canonico
10. R. D. Cheverton
11. J. M. Corum
12. W. R. Corwin
13. W. B. Cottrell
14. J. R. Dougan
15. W. L. Greenstreet
16. R. C. Gwaltney
17. P. P. Holz
18. S. K. Iskander
19. K. K. Klindt
20. J. G. Merkle
21. C. A. Mills
22. S. E. Moore
23. F. R. Mynatt
24. D. J. Naus
25. F. H. Neill
26-27. J. L. Rich
28. G. C. Robinson
29. G. M. Slaughter
30. J. E. Smith
31. W. J. Stelzman
32. H. E. Trammell
33-37. G. D. Whitman
38. Patent Office
39. Central Research Library
40. Document Reference Section
41-42. Laboratory Records Department
43. Laboratory Records (RC)

External Distribution

44. C. Z. Serpan, Reactor Safety Research, Nuclear Regulatory Commission, Washington, DC 20555
45. M. Vagins, Reactor Safety Research, Nuclear Regulatory Commission, Washington, DC 20555
46. Office of Assistant Manager for Energy Research and Development, DOE, ORO, Oak Ridge, TN 37830
47-48. Technical Information Center, DOE, Oak Ridge, TN 37830
49-478. Given distribution as shown in category RF (NTIS — 10)

☆U.S. GOVERNMENT PRINTING OFFICE: 1980-640-245/397